HHS Public Access

Author manuscript

Cell Metab. Author manuscript; available in PMC 2025 January 02.

Published in final edited form as:

Cell Metab. 2024 January 02; 36(1): 144–158.e7. doi:10.1016/j.cmet.2023.11.010.

ChREBP is activated by reductive stress and mediates *GCKR*-associated metabolic traits

Charandeep Singh[1,2,*], **Byungchang Jin**[1,2,*], **Nirajan Shrestha**[1,2], **Andrew L. Markhard**[3], **Apekshya Panda**[3,4,5], **Sarah E. Calvo**[3,4,5], **Amy Deik**[4], **Xingxiu Pan**[6], **Austin L. Zuckerman**[6,7], **Amel Ben Saad**[8], **Kathleen Corey**[1], **Julia Sjoquist**[1], **Stephanie Osganian**[1], **Roya Amini Tabrizi**[9], **Eugene P. Rhee**[2,10], **Hardik Shah**[9], **Olga Goldberger**[3], **Alan C. Mullen**[8], **Valentin Cracan**[6,11], **Clary B. Clish**[4], **Vamsi K. Mootha**[3,4,5], **Russell P. Goodman**[1,2,#]

[1]Liver Center, Division of Gastroenterology, Massachusetts General Hospital, Boston, MA 02114, USA

[2]Endocrine Unit, Massachusetts General Hospital, Boston, MA 02114, USA

[3]Howard Hughes Medical Institute and Department of Molecular Biology, Massachusetts General Hospital, Boston, MA 02114, USA

[4]Broad Institute of MIT and Harvard, Cambridge, MA 02142, USA

[5]Department of Systems Biology, Harvard Medical School, Boston, MA 02115, USA

[6]The Scintillon Institute, San Diego, CA 92121, USA

[7]Program in Mathematics and Science Education, University of California San Diego and San Diego State University, San Diego, CA 92093, USA

[8]Division of Gastroenterology, University of Massachusetts Chan Medical School, Worcester, MA 01655, USA

[9]Metabolomics Platform, Comprehensive Cancer Center, The University of Chicago, Chicago, IL 60637, USA

[10]Nephrology Division, Massachusetts General Hospital, Boston, MA 02114, USA

[11]Department of Chemistry, The Scripps Research Institute, La Jolla, CA 92037, USA

[#]**Correspondence and Lead Contact:** rpgoodman@mgh.harvard.edu (R.P.G.).

[*]These authors contributed equally to this work.

AUTHOR CONTRIBUTIONS

R.P.G. supervised the study. C.S., B.J., N.S., V. K.M., and R.P.G. designed experiments. C.S., B.J., N.S., A.L.M, and R.P.G performed experiments. A.P. and S.E.C. assisted with data analysis. C.S., B.J and R.P.G analyzed results and wrote the manuscript. K.C. and J.S. obtained and provided human clinical samples. A.C.M. and A.B.S. assisted with interpretation of data. H.S., C.B.C, and A. D. assisted with metabolomics experiments. O. G. assisted with mouse work and mouse colony management. V.C., X.P. and A.L.Z. provided the *Ec*STH tool. All authors read and edited the manuscript.

DECLARATION OF INTERESTS

V. K. M. and V. C. are listed as inventors on a patent application filed by Massachusetts General Hospital on the therapeutic uses of *Lb*NOX. V. K. M. is a scientific advisor to and receives equity from 5AM Ventures. A.C.M. received research support from Boehringer Ingelheim and GlaxoSmithKline for other projects not related to this work.

SUMMARY

Common genetic variants in glucokinase regular (*GCKR*), which encodes GKRP, a regulator of hepatic glucokinase (GCK), influence multiple metabolic traits in genome-wide association studies (*GWAS)* making *GCKR* among the most pleiotropic GWAS loci in the genome. It is unclear why. Prior work has demonstrated *GCKR* influences the hepatic cytosolic NADH/NAD^+ ratio, also referred to as reductive stress. Here we demonstrate that reductive stress is sufficient to activate the transcription factor ChREBP, and necessary for its activation by the GKRP-GCK interaction, glucose, and ethanol. We show that hepatic reductive stress induces *GCKR* GWAS traits such as increased hepatic fat, circulating FGF21, and circulating acylglycerol species, which are also influenced by ChREBP. We define the transcriptional signature of hepatic reductive stress and in humans show its upregulation in fatty liver disease and downregulation after bariatric surgery. These findings highlight how a *GCKR*-reductive stress-ChREBP axis influences multiple human metabolic traits.

Graphical Abstract

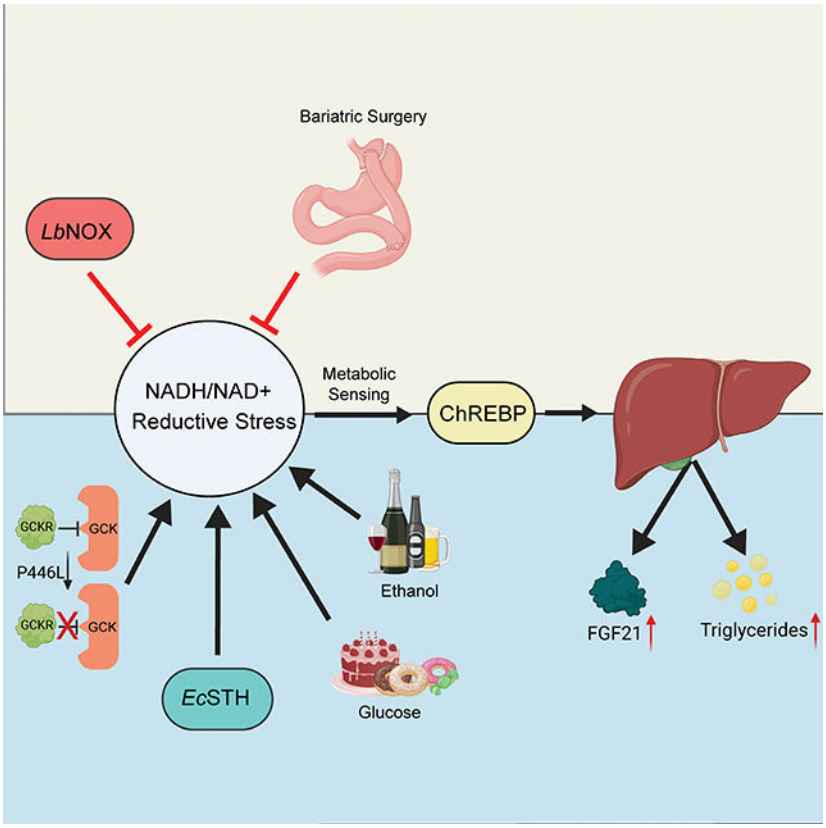

eTOC blurb

Singh *et al* find that increased hepatic cytosolic NADH/NAD+ activates the transcription factor ChREBP. This pathway underlies some metabolic traits associated with common *GCKR* genetic variants, such as circulating FGF21 and triglyceride levels, and likely more generally influences certain deleterious metabolic traits in humans.

INTRODUCTION

Over 100 human traits and diseases are linked to a single glucokinase regulator (*GCKR*) allele, making it among the most pleiotropic loci in the genome. Despite this, the mechanism underlying these associations remains largely unclear[1].

GCKR encodes glucokinase regulatory protein (GKRP), a predominantly liver-expressed protein which was first identified as a regulator of hepatic glucokinase (GCK) activity[2]. GCK is a low-affinity hexokinase whose biochemical catalytic activity is the phosphorylation of glucose to glucose-6-phosphate and which functions as a glucose sensor in multiple tissues including the pancreas, pituitary gland, and liver. During fasting, GKRP sequesters GCK in the nucleus to prevent a futile metabolic cycle caused by the simultaneous activity of both GCK and glucose-6-phosphatase (G6PC), the first step of glycolysis and the last of gluconeogenesis, respectively[3].

With the advent of genome-wide-association studies (GWAS), common genetic variants in *GCKR* were among the first genetic loci to be associated with increased risk of diabetes[4]. This was attributed to the rs1260326 *GCKR* variant, which encodes a P446L missense variant in GKRP that has been shown to influence GKRP's inhibition of glucokinase, resulting in higher GCK activity and hepatic glucose uptake[5]. This led to multiple efforts to drug the GCKR-GCK interaction or target GCK activation as potential antidiabetic treatments, owing to their common property of decreasing circulating glucose.

Subsequent GWAS studies have demonstrated a remarkable number of other diverse traits linked to *GCKR* rs1260326, including multiple blood metabolites, diseases such as fatty liver disease[6] and gout[7], circulating levels of FGF21[8], behavioral traits such as coffee[9] and alcohol consumption[10], among over 100 other traits[1]. In recent work we demonstrated that *GCKR* influences the hepatic NADH/NAD^+ redox potential (NADH reductive stress), and that modulation of hepatic reductive stress could influence many traits associated with *GCKR* variants, such as plasma FGF21 levels, through an unclear mechanism[1].

Here, we provide evidence that *GCKR's* metabolic pleiotropy can in part be explained via the action of the transcription factor ChREBP (gene name *MLXIPL*). ChREBP was first identified as a hepatic transcription factor that was responsive to alterations in glucose levels in an insulin-independent manner[11], and has subsequently been shown to also be activated by fructose[12], glycerol[13], and ethanol[14], though the precise metabolic underpinnings of its regulation remain unclear.

We demonstrate the dependence of the activation of ChREBP on changes in cytosolic NADH/NAD^+ by using a combination of four experimental methods applied *in vitro* and/or *in vivo*: 1) expression of *Lb*NOX[15], a bacterial enzyme which lowers NADH/NAD^+; 2) expression of *Ec*STH [16], a bacterial enzyme which raises NADH/NAD^+; 3) ethanol gavage, which raises NADH/NAD^+; and 4) manipulation of extracellular lactate/pyruvate ratios which are in equilibrium with cytosolic NADH/NAD^+. We show that increased cytosolic NADH/NAD^+ is sufficient for ChREBP activation and necessary for its activation by ethanol, glucose, and inhibition of the GKRP-GCK interaction. We define the *in vivo* hepatic transcriptional signature of reductive stress and demonstrate it is largely mediated

by ChREBP activation. We also find that metabolic traits associated with *GCKR* genetic variants are influenced by ChREBP. We extend our observations to human disease showing that hepatic reductive stress, reflected in blood levels of the hepatic NADH/NAD^+ biomarker α-hydroxybutyrate (αHB), and the transcriptional signature of reductive stress are metabolic features of patients with non-alcoholic fatty liver disease (NAFLD), suggesting reductive stress-dependent ChREBP activation as a cardinal feature of common human metabolic disease.

RESULTS

Hepatic reductive stress alters the liver transcriptome

In prior work we used ethanol gavages and hepatic expression of *Lactobacillus brevis* H_2O-forming NADH oxidase (*Lb*NOX), to raise and lower the hepatic cytosolic NADH/NAD^+ ratio (Fig. 1A–C)[1]. In this model, we previously reported that ethanol-induced upregulation of circulating FGF21 was entirely dependent on elevated hepatic reductive stress[1], which in subsequent experiments we found to correlate with hepatic FGF21 mRNA levels in unpublished data. To comprehensively characterize how hepatic reductive stress altered the hepatic transcriptome, we first performed RNA sequencing (RNA-Seq) on the mice livers from this experiment and in a second experiment where we used adenovirus-mediated hepatic expression of a novel genetically encoded tool based on *E. coli* soluble transhydrogenase (*Ec*STH)[16]. *Ec*STH couples the oxidation of NADPH to the generation of NADH from NAD^+ and provides a second independent method in addition to ethanol of generating hepatic reductive stress (Fig. 1A–C)[16].

We identified 160 NADH/NAD^+ responsive genes as those genes whose expression was increased by ethanol but not ethanol and *Lb*NOX together, and which were additionally increased with hepatic *Ec*STH expression (Fig. 1D; Supplemental Table 1; See Methods). Examples of such genes include the hepatokine *Fgf21*, which has pleiotropic effects on organismal metabolism[17], Acetyl-CoA carboxylase (*Acaca*), a rate-limiting enzymatic step in *de novo* lipogenesis, and *Pnpla3*, a triacylglycerol lipase implicated in the pathogenesis of non-alcoholic steatohepatitis (Fig. 1E)[18].

We next confirmed that the transcriptional changes in our ethanol/*Lb*NOX experiment were not simply an artifact resulting from alterations in ethanol metabolism (Supplementary Fig. 1A). To confirm that it was alteration in NADH/NAD^+ but not ethanol or its other downstream metabolites that were responsible for the observed transcriptional changes, we measured αHB and acetate in both our *Lb*NOX/EtOH model and in an ethanol gavage model in the presence or absence of fomepizole, an alcohol dehydrogenase (ADH) inhibitor (Supplementary Fig. 1B–C). Only αHB, a biomarker of hepatic NADH/NAD^+[1], correlated with activation of NADH-responsive genes from our RNA-Seq dataset, and fomepizole inhibited both the generation of αHB by ethanol metabolism and activation of NADH/NAD^+-sensitive genes (Supplementary Fig. 1D–G).

ChREBP mediates reductive-stress dependent hepatic transcriptional changes

Our data led us to hypothesize the existence of an NADH/NAD$^+$-responsive transcription factor, which we aimed to identify via over enrichment analysis on our 160 mouse NADH/NAD$^+$-responsive genes using WebGesalt[19]. The top pathway identified was activation of ChREBP (gene name *Mlxipl*), a lipogenic glucose- and ethanol-responsive transcription factor (Fig. 2A)[20]. To confirm ChREBP mediated the NADH/NAD$^+$-dependent transcriptional changes in our system we performed RNA-Seq on the livers of ethanol (EtOH)-gavaged wildtype and ChREBP knockout (KO) mice and compared this to our *Lb*NOX/EtOH and *Ec*STH RNA-Seq data sets. We first examined transcript levels of several known ChREBP targets[12,21] (Fig. 2B), which demonstrated a pattern consistent with ChREBP-dependent activation in both data sets, as did a comparison of the NADH-responsive gene set from Figure 1D in our *Lb*NOX/EtOH and ChREBP-KO/EtOH gene sets (Fig. 2C). A comparison of genes in each experiment whose activation via alcohol was prevented by either *Lb*NOX or ChREBP KO overlapped significantly ($p < 1e\text{-}5$, Fig. 2D), with a majority of transcripts requiring ChREBP to be upregulated by reductive stress. *MLXIPL* was further highly ranked using transcription factor enrichment analysis[22] of this overlapping set (rank 3/1632, Fig. 2E) though not in the non-overlapping set (Fig. 2F). Together, these data confirm *in vivo* NADH/NAD$^+$-mediated activation of hepatic ChREBP. We note that as not all reductive-stress responsive transcripts were ChREBP-dependent, it is possible other transcription factors might contribute to the transcriptional signature of reductive stress.

ChREBP is activated by reductive stress

To confirm elevated cytosolic NADH/NAD$^+$ activates ChREBP, we first measured ChREBP activation in primary hepatocytes with different cytosolic NADH/NAD+ levels. Since cytosolic NADH/NAD$^+$ is in equilibrium with the external lactate/pyruvate (L/P) ratio[23], we perturbed the system by "clamping" it with different quantities of lactate and pyruvate in the media (Fig. 3A–C). We observed that higher cytosolic NADH/NAD$^+$ ratios resulted in higher αHB production (Fig. 3B), consistent with our prior observation that αHB is a biomarker of hepatic cytosolic NADH/NAD$^+$[1]. It also resulted in increased ChREBP transcript abundance (Fig. 3C).

We then confirmed these findings in a second cellular system employing a luciferase reporter system measuring ChREBP activity via insertion of a synthetic construct of three sequential carbohydrate response elements (ChoREs) upstream of luciferase gene expression (Fig. 3D). Expression of ChREBP (Fig. 3E), along with MLX, ChREBP's heteromeric partner, was sufficient to activate the reporter system (Fig. 3F), which was additionally responsive to glucose media levels (Fig. 3G). *Lb*NOX expression in our reporter system, which lowers the intracellular NADH/NAD$^+$ ratio as reflected in a lowered lactate/pyruvate ratio (Fig. 3H), resulted in markedly lower ChREBP activity (Fig. 3I). As an alternative method to increase the NADH/NAD$^+$ ratio, we used *E. coli* soluble transhydrogenase (*Ec*STH). In our system, this both increased the lactate/pyruvate ratio (Fig. 3J) and increased ChREBP activity (Fig. 3K). Together, these data indicate that an elevated cytosolic NADH/NAD$^+$ ratio is both necessary and sufficient to activate ChREBP.

ChREBP activation via reductive stress correlates with increased intracellular triosephosphates

The precise metabolic mechanism underlying ChREBP activation is unclear, though is generally assumed to be via alterations in the abundance of an intracellular metabolite that influences ChREBP activity either directly or indirectly. Multiple candidates have been proposed including xylulose-5-phosphate (X5P)[24], glucose-6-phosphate (G6P)[25,26], fructose 2,6-bisphosphate[27], and more generally hexose-phosphate and triose-phosphate pools[13,28]. To examine how reductive stress influences these metabolites, we performed a combination of targeted and untargeted intracellular metabolomics on HEK 293T cells in which ChREBP activity was perturbed in five different ways with a combination of GCK, *Lb*NOX, and *Ec*STH expression (Fig. 4A and 4B). We then calculated correlation of ChREBP activation with the relative abundance of approximately 270 intracellular metabolites using LC-MS measurements, as well as a GC-MS protocol optimized for measurement of sugar phosphates such as G6P and Xu5P. These sugar phosphates are difficult to distinguish from isomers such as fructose-6-phoshate and pentose/pentulose-5-phosphate on HILIC-MS platforms due to retention time overlap and identical fragmentation patterns [Supplementary Table 2]. We found the triosephosphates glyceraldehyde-3-phosphate (GAP) and glycerol-3-phosphate (G3P) were among the top metabolites correlated with ChREBP activity, as was NADH and Fructose 1,6-bisphosphate (Fig. 4C–F). In contrast, we did not find the sugar phosphates G6P and X5P (Fig 4G–H) well correlated with ChREBP activity. Both GAP and G3P have clear links to cytosolic NADH/NAD^+ via the activities of glyceraldehyde-3-phosphate dehydrogenase (GADPH) and glycerol-3-phosphate dehydrogenase (GPDH) (Fig. 4I). Our data suggest reductive stress may activate ChREBP via increased perturbation of phosphate ester glycolytic intermediates through NADH/NAD^+ modulation of the activity of GAPDH and/or GPDH.

A *GCKR-GCK* axis activates ChREBP in an NADH/NAD^+-dependent manner

A common *GCKR* P446L variant increases hepatic NADH/NAD^+ as evident by its association with increased serum αHB levels in humans[29], and in prior work we demonstrated that *GCKR* expression altered the hepatic NADH/NAD^+ ratio, likely as a result of alterations in GCK activity [1]. This led us to hypothesize that modulation of the *GCKR-GCK* axis could influence ChREBP activity via alterations in the hepatic NADH/NAD^+ ratio which we tested in three different cellular systems.

We first tested this in the hepatocyte cell line HepaRG, a hepatic progenitor cell line with the ability to differentiate into hepatocyte-like and biliary-like cells with close functional resemblance to primary human hepatocytes which has been used in the functional metabolic characterization of steatosis and fibrosis[30,31]. We confirmed *GCKR* overexpression decreased cellular cytosolic NADH/NAD^+, as evidenced by decreased media lactate/pyruvate, (Fig. 5A), with a corresponding decrease in ChREBP transcript abundance (Fig. 5B).

We next examined the relationship between ChREBP activity and GCK and *Lb*NOX expression in our luciferase reporter system in the HEK293T cell line. We found that GCK

expression increased ChREBP activity, though this was prevented by simultaneous *Lb*NOX expression (Fig. 5C).

Finally, we tested the effect of the *GCKR* SNP rs120326 (P446L) on the expression of our NADH/NAD$^+$ responsive gene set in a previously reported RNAseq data from a large set of human liver biopsies (Fig. 5D)[32] and from human liver organoids derived from iPSC cells with different *GCKR* genotypes (Fig. 5E) [33]. We found significant enrichment of our gene set, confirming the transcriptional impact of this common variant.

*Ec*STH and ChREBP activity influence *GCKR*-associated metabolic traits

Our data led us to hypothesize that some *GCKR*-associated metabolic traits identified through GWAS studies might be attributable to reductive stress mediated ChREBP activation, which we tested with our GFP/*Ec*STH and EtOH/ChREBP *in vivo* experiments. We focused on FGF21 and lipid traits which we had previously demonstrated were downstream of hepatic reductive stress[1] and confirmed that reductive stress induced by *Ec*STH was sufficient to induce an increase in circulating FGF21 levels and hepatic fat accumulation (Fig 6A, C). We further found that ethanol's influence on FGF21 was entirely dependent on ChREBP (Fig 6B) and partially dependent on its influence on total hepatic triglycerides (Fig. 6D). We measured the effect of ChREBP on ethanol's ability to influence multiple specific triglycerides and diacylglycerides species, some of which (e.g. TAG 48:2, TAG 48:3, and DAG 34:1) are formally associated with *GCKR* in GWAS studies[29], and in each case found a direction consistent with human *GCKR* genetics (Fig 6E–H). We note that ChREBP knock-out was unable to fully prevent ethanol's increase in nearly all TAG and DAG species abundance. We speculate this may be related to the activity of delta-5 and delta-6 desaturates (D5D/D6D), which increase the abundance of TAG and DAG species containing double bonds with increases in the cytosolic NADH/NAD$^+$ ratio[34]. This activity would be expected to be increased by ethanol (a source of NADH) but not influenced by ChREBP.

Not all *GCKR*-associated traits we tested could be explained via ChREBP activation. For example, multiple glycerophospholipid species, such as phosphatidylcholines and phosphatidylethanolamines, are associated with human *GCKR* genetic variation[29,35], but these specific lipid traits did not appear to be influenced via reductive stress or ChREBP (Supplementary Figure 2), suggesting they were instead influenced by ChREBP-independent metabolic effects of the GKRP-GCK interaction.

Metabolic traits associated with *GCKR*, *MLXIPL*, and *FGF21* genetic variants overlap

Because our data outline a causal chain from *GKCR* to *MLXIPL* to *FGF21*, we revisited existing GWAS data to assess to what extent these loci demonstrate similar trait associations. To do this we utilized the Type 2 Diabetes Knowledge Portal[36] which aggregates genetic datasets related to Type 2 Diabetes and associated traits. We found substantial overlap, with nearly two-thirds (58/89) of traits associated with *GCKR* also associated with *MLXIPL,* and a majority of *FGF21* traits also being associated with both *MLXIPL* and *GCKR* (Fig. 6I).

Whereas certain *GCKR*-associated metabolic traits such as hepatic triglycerides have clear links to the liver, others such as the renal function marker cystatin C or platelet size do not.

Our results raise the possibility that some of these other, extra-hepatic *GCKR* associated traits could be mediated through its effect on FGF21. Although we acknowledge that experimental validation is required, we note that the directionality of effects in GWAS is internally consistent.

The transcriptional signature of hepatic reductive stress is present in patients with fatty liver disease

Having demonstrated that *GCKR* loss-of-function activates ChREBP via alterations in hepatic NADH/NAD^+, we hypothesized that hepatic reductive stress might represent a metabolic mechanism for hepatic fat accumulation in humans. To test this, we first measured circulating αHB, a liver-specific biomarker of elevated hepatic reductive stress[1,37], in patients with non-alcoholic fatty liver disease (NAFLD) in a well-characterized patient cohort. We found αHB was significantly elevated compared to healthy controls (Fig. 7A). Elevated reductive stress was also associated with increased FGF21 and circulating triglycerides, which are established clinical associations with NAFLD [38] (Fig. 7B–C) and consistent with our findings in mice. We then analyzed previously published hepatic RNA-Seq data sets from patients with NAFLD for evidence of our transcriptional signature of reductive stress and found significant enrichment via GSEA[39,40] in 6 different data sets (Fig. 7D). This included ambulatory patients with and without NAFLD [41], patients who developed hepatic steatosis after liver transplantation[42], and patients before and after bariatric surgery [43], where circulating αHB is the top changing serum metabolite [44] and which generally improves or resolves NAFLD[45]. Together these data support a role for reductive stress in mediating metabolic traits associated with *GCKR* variants such as fatty liver, circulating triglycerides, and FGF21.

DISCUSSION

Motivated by the observation that circulating α-hydroxybutyrate (αHB) is a biomarker of hepatic cytosolic reductive stress, we previously demonstrated that *GCKR*, which has a common variant that influences circulating αHB, increases hepatic reductive stress[1]. With the use of *Lb*NOX, we were further able to demonstrate that certain metabolic traits associated with *GCKR* via GWAS studies could be influenced via reductive stress. The mechanistic underpinnings of how reductive stress can influence some of these traits is clear. For example, αHB is produced from α-ketobutyrate via LDH and coupled to the oxidation of NADH to NAD^+, and thus alterations in the NADH/NAD^+ levels would be expected to directly influence αHB[46]. How reductive stress can influence many other traits, such as circulating FGF21 levels, is less clear. In the current work we provide data to support the conclusion that multiple metabolic traits linked to *GCKR* are mediated by NADH/NAD^+-dependent activation of the transcription factor ChREBP. This is significant for several reasons.

First, it demonstrates a novel metabolic mechanism by which ChREBP activity is modulated. ChREBP is traditionally viewed as a carbohydrate-responsive transcription factor as it is activated by both glucose[11] and fructose[13], though it can also be activated by other metabolites such as ethanol[14] and glycerol[13]. Our data suggest that its activation

by glucose and ethanol is directly dependent on a common downstream elevation in cytosolic NADH/NAD^+. Importantly, as the cytosolic NADH/NAD^+ ratio is a central metabolic parameter that is coupled to multiple facets of hepatic metabolism[47], our findings greatly expand upon the metabolic contexts in which ChREBP activity might be influenced. We additionally found that perturbation of ChREBP activity in multiple ways, including via NADH/NAD^+ manipulation, leads to alterations in intracellular phosphates of which triosephosphates are among the highest correlated with ChREBP activity (Fig 4). Triosephosphates are linked to NADH/NAD^+ via GAPDH and GPDH (Fig. 4I) and are also the level at which other ChREBP activators, such as glycerol, enter the glycolytic carbon pool. Our data therefore supports the idea of triosephosphates as ChREBP activators as has been previously proposed[13], and links these metabolites to reductive stress. Interestingly, ChREBP itself may influence redox status as its deletion increases cytosolic NADH/NAD^+[48], which may suggest that ChREBP operates in a reductive stress feedback loop by lowering reductive stress when it becomes elevated.

Second, our findings help explain the metabolic pleiotropy of *GCKR*. *GCKR* encodes glucokinase regulatory protein (GKRP), a primarily liver-specific protein, which allosterically inhibits glucokinase during periods of fasting[49]. A common P446L missense variant in GKRP, which affects its inhibition of glucokinase activity[5], has been linked to over a hundred different GWAS associations. While this stems in part from the relatively high frequency of the rs1260326 *GCKR* variant, which approaches 50% in some populations[50], the breadth of *GCKR-associated* traits is difficult to explain by its canonical role as a regulator of hepatic glycolytic flux. We demonstrate here that NADH-dependent transcriptional activity of ChREBP likely mediates *GCKR*-associated traits such as FGF21 and certain lipid traits like circulating triglycerides, and our data suggest that it is a primarily transcriptional mechanism contributing to *GCKR*'s influence on triglycerides, rather than its predicted effects on malonyl-CoA, as originally proposed[5]. While the full extent to which *GCKR-associated* traits are due to ChREBP activation remains to be defined, we note that it is likely that some *GCKR*-associated traits, such as circulating glucose levels, are independent of ChREBP and a direct result of increased hepatic glycolysis mediated by *GCKR* variants. We further speculate that FGF21 may contribute to *GCKR* metabolic pleiotropy through its induction by ChREBP. FGF21 is a known ChREBP target[51], FGF21 is linked to *GCKR* via GWAS[8], reductive stress is sufficient to increase hepatic FGF21 levels (Fig 6), and ethanol's induction of FGF21 appears dependent on ChREBP (Fig 6). More importantly, FGF21 has been shown to influence traits that are associated with *GCKR* variants through human genetics. For example, *GCKR* influences measures of renal function like urinary sodium excretion[52] and glomerular filtration rate[53], which in a recent Mendelian randomization study was associated with a genetic proxied FGF21[54] and with internally consistent directional effects. *GCKR* variants also influence alcohol consumption[10], which has been shown to be directly modulated by FGF21[55].

Finally, our work suggests a role for reductive stress in human disease. Fatty liver disease is the most common form of liver disease in the world[56] and in its end stage is the leading indication for liver transplantation in the US[57]. Our data support the idea that reductive stress is a metabolic feature of NAFLD and, as alcohol metabolism is a robust source of hepatic reductive stress, it is likely a shared causal mechanism contributing to both alcohol

and non-alcohol related fatty liver disease and is further a likely metabolic contributor to the elevated triglycerides and circulating FGF21 seen in both conditions[38,58] via activation of ChREBP. As such, therapeutically targeting hepatic reductive stress might prove to be a novel strategy to target hepatic fat accumulation from both alcohol and non-alcohol causes. We also note that our work provides a potential mechanism linking SLC16A11 to metabolic disease. A type 2 diabetes risk haplotype in SLC16A11 confers a substantial (~20%) increased diabetes risk in Mexico[59], and the risk haplotype has been shown to increase the cytosolic NADH/NAD^+ ratio[60]. SLC16A11's activation of ChREBP via an increased cytosolic NADH/NAD^+ ratio could plausibly influence hepatic insulin resistance and diabetes risk via modulation of ChREBP activity[61].

An additional outstanding question is the underlying source of elevated hepatic stress in patients with NAFLD, and the mechanism underlying lower reductive stress after bariatric surgery. We speculate that obesity itself could increase hepatic reductive stress via increased delivery of free fatty acids to the liver in the setting of excess adiposity, which through β-oxidation would be a direct source of elevated hepatic NADH, though this remains to be proven.

In sum, by directly manipulating cytosolic NADH/NAD^+ *in vivo* with *Lb*NOX, the new genetic tool *Ec*STH, ethanol oxidation, and clamped lactate/pyruvate ratios, we have demonstrated that this critical metabolic parameter influences the activity of the transcription factor ChREBP, which in turn influences multiple metabolic traits. This NADH/NAD^+-ChREBP axis can be influenced in multiple ways: through human genetics via common *GCKR* polymorphisms; through consumption of alcohol; and likely through risk factors for non-alcoholic fatty liver disease such as obesity. Together, our work adds to the growing evidence for the importance of reductive stress as a critical metabolic parameter influencing human metabolism and disease.

Limitations of the Study

Our data does not address well-established physiologic and genetic influences on NADH/NAD^+ biology and hepatic physiology which may have important effects on a GCKR-NADH/NAD^+-ChREBP axis. For example, circadian rhythms influence both the hepatic transcriptome[62] and redox state[63], and glucose levels can influence GCK expression[64], which would make feeding/fasting status an important variable in our data. We also note that the C57BL/6J strain used in our work lack nicotinamide nucleotide transhydrogenase (NNT), which influences cellular redox state[65] and may contribute to metabolic differences between the C57BL/6N and C57BL/6J strains. As such, future studies examining differences in reductive stress and ChREBP biology between these strains are warranted.

Second, our work does not fully account for the metabolic or transcriptional effects of reductive stress. It appears for example that not all genes induced by reductive stress can be attributed to ChREBP activation (Fig. 2D), nor does ChREBP appear to entirely mediate *GCKR* associated traits that are increased by ethanol outside of FGF21, which suggests ChREBP-independent effects of reductive stress. This is not surprising given transcriptional changes due to alterations in metabolite levels are multifactorial, and there are established mechanisms linking NADH/NAD^+ biology to transcription outside of

ChREBP. For example, sirtuins are important regulators of transcription and SIRT1 activity appears to be influenced by both local variations of NAD^+ concentrations in the nucleus[66] and variations in NADH levels linked to circadian cycles[67].

Changes in mitochondrial redox metabolism have been linked to changes in histone acetylation, methylation, and gene transcription[68], and reductives stress could plausibly influence the epigenome.

We also note that our intracellular metabolomics screen for metabolites correlated with ChREBP activation was performed in a 293T cell line which is expected to have significant metabolic differences compared to hepatic metabolism *in vivo*, particularly with native *GCKR* or *GCK* expression and pentose phosphate pathway metabolism. It is thus possible that metabolic activation of ChREBP in these different contexts (cell culture versus in the liver *in vivo*) could differ.

Finally, while we have demonstrated that reductive stress is sufficient to activate ChREBP, the precise mechanism underlying its activation is unclear. Our work supports the established idea that ChREBP senses changes in abundance of phospho-ester glycolysis intermediates, and we have linked reductive stress induced ChREBP activation in particular to the abundance of F1/2–6BP, GAP, and G3P, with GAP showing the highest correlation with ChREBP activity, though further efforts will be required to elucidate the mechanism linking these intermediates to ChREBP activation.

STAR METHODS

RESOURCE AVAILABILITY

Lead contact—Further information and requests for resources and reagents should be directed to and will be fulfilled by the Lead Contact, Russell Goodman (rpgoodman@mgh.harvard.edu).

Materials availability—No unique reagents were generated in this study. Certain materials are shared with academic and non-profit research organizations for research only under an MTA.

Data and code availability

- RNA-seq data have been deposited at GEO under accession numbers GSE227264, GSE227057, and GSE237068, and are publicly available as of the date of publication.
- This paper does not report original code.
- Any additional information required to reanalyze the data reported in this paper is available from the lead contact upon request.

EXPERIMENTAL MODEL AND SUBJECT DETAILS

Animal Studies—All animal experiments were approved by the Massachusetts General Hospital Institutional Animal Care and Use Committee, and all relevant ethical regulations

were followed. Unless otherwise noted, all mice were group-housed and age-matched with access to administered chow (Prolab Isorpro RMH 3000 5p75) and water ad libitum in a pathogen-and temperature controlled room with a 12h:12h light-dark cycle, and sacrificed after a 4–6 hour AM fast with isoflurane anesthesia for euthanasia.

ChREBP KO mice, originally described in Iizuka et al 2004[12], were obtained from the Jackson Laboratory (strain #010537; RRID:IMSR_JAX:010537). Experiments involving ChREBP KO mice used both male and female mice. All other mice were male C57BL/6J (strain #000664; RRID:IMSR_JAX:000664) mice aged 7–16 weeks purchased from The Jackson Laboratory unless noted otherwise.

The Figure 1 experiment involving alcohol gavages after *Lb*NOX or luciferase adenoviral tail vein injections were previously described[1]. For hepatic *Ec*STH and GFP expression, mice were retro-orbitally injected with $2E^9$ PFU adenovirus (Vector Biolabs) and sacrificed four days later.

For alcohol or water gavage experiments, an oral gavage 3.5 g/kg of alcohol or equivalent H_2O per body weight was given at the start of the experiment, followed by a second gavage of half the initial dose 1 h later. Mice received IP injections of fomepizole of 15 mg/kg 30 minutes before and 7.5 mg/kg 90 and 150 minutes after the initial gavage or equivalent volume H_2O for controls. Plasma and liver tissue were collected 4–6 hours after initial gavage under isoflurane anesthesia and stored at −80°C (plasma) or flash frozen in liquid nitrogen (liver) until further processing.

Primary Hepatocyte Experiments—Primary hepatocytes were isolated as previously described[1]. Briefly, primary hepatocytes were freshly isolated by hepatic perfusion and enzymatic digestion with Liberase TM (Sigma-Aldrich) followed by plating in six-well collagen-coated plates at a density of 4×10^5 cells per well prior to subsequent experiments.

HepaRG cell culture—Undifferentiated HepaRG cells lines were purchased from Biopredic International.

Undifferentiated cell lines were infected with GFP or *GCKR* overexpressing lentiviruses to have a stable expression of the gene of interest and passaged before using for actual experiments. Undifferentiated HepaRG cells were cultured in Williams E media supplemented with ADD711 supplement (Biopredic International) and 1% PenStrep (This media composition is referred to as proliferation media). These cells were maintained in this media for 14 days with media change every 1–2 days. Cells were differentiated by changing the media to 50% proliferation media and 50% of differentiation media. Differentiation media was prepared supplementing Williams E media with ADD721 and 1% Pen-Strep. After one day, media was changed to 100% differentiation media and maintained for 14 days to reach hepatocyte-like function. On the last day, media was again changed to 100% differentiation media and cells were allowed to grow for 24h before harvesting the RNA for the RT-qPCR experiments and media for metabolomics experiments. *GCKR* transcript CCDS1757.1 was PCR flanked and amplified using Fwd 5’ TTAGTGAACCGTCAGATCCGCATGCCAGGCACAAAACGGT 3’ and Rev 5’

TTGTCTCGAGGTCGAGAATTTCACTGAACGTCAGGCTCTA 3'. The amplified product was cloned into pLJM1 empty vector using NEBuilder HiFi DNA assembly cloning kit (New England Biolabs). pLJM1-Empty was a gift from Joshua Mendell (Addgene plasmid # 91980).

Human studies—Blood samples from patients with NAFLD were obtained from the MGH NAFLD Cohort Registry which has been previously described[70]. In this cohort, blood samples and liver biopsies were obtained from patients undergoing bariatric surgery and hepatic fat accumulation was diagnosed on liver biopsy. Healthy controls were taken from the Partners Healthcare Biobank from patients with a Charlson Index of 0, the absence of diabetes, normal serum alanine aminotransferase (ALT), normal serum triglycerides, and a BMI between 18–25. All studies were approved by the Mass-General Brigham institutional review board and all participants provided written informed consent.

METHOD DETAILS

RNA sequencing and downstream analyses—RNA sequencing on livers from the Figure 1D experiment was performed at the Harvard University Biopolymers Facility for the *Lb*NOX/ethanol and ChREBP mice, and through Novogene for the *Ec*STH/GFP experiment. Briefly, total liver RNA was isolated from frozen liver tissue with RNeasy mini kits (Qiagen). For the *Lb*NOX/ethanol and ChREBP/ethanol experiments, mRNA was isolated with KAPA mRNA HyperPrep kit (Illumina) and sequenced on an Illumina NextSeq 500 (Harvard Biopolymers Facility). For the *Ec*STH/GFP experiment, mRNA was isolated with the NEBNext Ultra II RNA Library Prep Kit for (Illumina) and sequenced on a NovaSeq 6000 (Novogene). All RNAseq samples were aligned to the mouse reference genome (GRCm38 mm10) using Salmon 1.5.1[71], followed by count normalization and subsequent analysis with DESeq2 1.38.3[72]. Sequencing data are available at Gene Expression Omnibus GSE227264, GSE227057, and GSE237068.

For the identification of NADH/NAD^+ responsive genes in Figure 1D we first calculated all significantly changing genes in the *Lb*NOX/EtOH experiment (DESeq2, adjusted p<=0.05, n= 2038 genes). We then clustered these genes to find co-expressed modules (pheatmap R package v. 1.0.12 with row-normalized data with scaling), then identified the single cluster of genes that increased expression with ethanol but not the ethanol+*Lb*NOX condition (n=831 genes). We then filtered these 831 genes (increased with ethanol but not ethanol + *Lb*NOX) to those that additional increased with *Ec*STH expression *in vivo* compared to GFP (DESeq2, p <0.05, n=1560), yielding 160 NADH/NAD^+ responsive genes.

ChREBP/EtOH responsive genes (Figure 2D) were identified in the same manner as NADH/NAD+ responsive gene in the *Lb*NOX/EtOH experiment. We first calculated all significantly changing genes in the ChreBP/EtOH experiment (DESeq2, adjusted p<=0.01, n= 1296 genes), identified co-expressed modules using pheatmap, and identified the cluster of genes that increased expression with ethanol but not with ethanol+ChREBP KO (n=543 genes). For enrichment analysis (Figure 2A), we performed over-representation Analysis (ORA) via WEB-based Gene SeT AnaLysis Toolkit 2019 (WebGestalt; https://www.webgestalt.org/[73])

using the Reactome database (Version 66, September 2018). The input gene set was our 160 NADH/NAD+ responsive genes using the illumina mouseref 8 background (n=25,697).

Transcription factor enrichment analysis (Figure 2E–F) was performed using ChIP-X Enrichment Analysis Version 3 (ChEA3)[22] using the indicated gene sets and the top rank integrated results. The *p* value for the overlap of ChREBP/EtOH and NADH/NAD^+-responsive genes in Figure 2D was calculated using Chi square.

qPCR—For qPCR experiments in Supplementary Figure 1, RNA was isolated using a Qiagen RNAeasy kit (Qiagen) and reverse transcribed using the SuperScript III First-Strand Synthesis System (Invitrogen) or iScript gDNA clear cDNA sythesis kit (Biorad). Quantitative PCR was performed using an Applied Biosystems 7500 Fast Real-Time PCR system, using the following primers from Thermo Fisher Scientific: G6pc (Mm00839363_m), Fasn (Mm00662319_m1) and Acaca (Mm01304257_m1). Hprt (Mm03024075_ m1) was used as an internal control. The remaining qPCR experiments were performed on a Thermo Quant Studio 6 PCR system with the following custom-designed qPCR primers:

Human ChREBP Fwd: 5'-CAGACAGCAACAAGACCGAG-3'

Human ChREBP Rev: 5'-GTCAAACCCCAGCTTGATGT-3'

Human GAPDH Fwd: 5'-GCTCTCTGCTCCTCCTGTT-3'

Human GAPDH Rev: 5'-GCGCCCAATACGACCAAAT-3'

Human β-actin Fwd: 5'-AGAAAATCTGGCACCACACC-3'

Human β-actin Rev: 5'-AGCACAGCCTGGATAGCAA-3'

Mouse β-actin Fwd: 5'-TACTCTGTGTGGATCGGTGG-3'

Mouse β-actin Rev: 5'-TCGTACTCCTGCTTGCTG AT-3'

Mouse HPRT and ChREBP QuantiTech primer assays used were purchased from Qiagen (Mm_Hprt_1_SG QT00166768 and Mm_wbscr14_1_SG QT00125335 respectively) Applied Biosystems TaqMan Fast Advanced Master Mix or Itaq™ Universal SYBR were used in the qPCR experiments, following quantities recommended by Vendors.

Lentivirus production—Human *GCKR* and GFP overexpression lentiviruses were prepared by transfecting VSV-G, psPAX2 and pLYS6-*GCKR* or plys6-GFP plasmids together into HEK293T cells. Virus particles were collected by filtering the supernatant from HEK293T cultures through 0.45 μm syringe filter.

Luciferase Reporter Assays and Plasmid Construction—For pcDNA3.1-ChREBPα and pcDNA3.1-Mlxγ, Mouse ChREBPα (accession number NM_021455.5) and mouse Mlx (accession number NM_011550.3) were synthesized by GENEWIZ (Suzhou, China) and cloned into pcDNA3.1 (Invitrogen). pcDNA3.1-eGFP was purchased from

Addgene (Plasmid129020)[1]. pcDNA3.1-*Lb*NOX was generated by subcloning *Lb*NOX (Addgene plasmid 75275) into pcDNA3.1 (Invitrogen). *Ec*STH was subcloned into pCDNA3.1 (Invitrogen) from pLVX-TetOne-Puro-EcSTH[16]. pGL4.14[luc2/Hygro]-ChoRE was generated via gene synthesis of a construct containing three consecutive mouse carbohydrate response elements (ChoRE) and the minimal LPK promoter [74](ATGGACGCCACGGGGCACTCCCGTGGTTCCTATGGACGCCACGGGGCACTCCC GTGGTTCCTATGGACGCCACGGGGCACTCCCGTGGTTCCTAGGCCCCATCCCACT GACAAAGGCA GAGTATAAAGCAGACCCACAGACACAGCAGGTACGCAGCA) which was cloned upstream of *Photinus pyralis* luciferase reporter gene in pGL4.14 (Promega). GCK transcript CCDS5479.1 was PCR flanked and amplified using Fwd 5' TTAGTGAACCGTCAGATCCGATGCTGGACGACAGAGCCAGGA 3' and Rev 5' CTTGTACCCGGTAGCGCTAGTCACTGGCCCAGCATACAGGCC 3'. The amplified product was cloned into PLJM1 empty vector (Addgene) with the help of NEBuilder HiFi DNA assembly cloning kit (New England Biolabs). pLJM1-Empty was a gift from Joshua Mendell (Addgene plasmid # 91980).

To assay ChREBP's activity with the luciferase assay kit, HEK293T cells were seeded into 24 well plates for 24 hours before transfection. The next day, cells were co-transfected with the indicated combination of pcDNA3.1-ChREBPα, pcDNA3.1-Mlxγ, pGL4.14[luc2/Hygro]-ChoRE, pGL4.75[hRluc/CMV], PLJM1-hGCK, pcDNA3.1-*Lb*NOX, pcDNA3.1-EcSTH, or pcDNA3.1-GFP plasmids. Lipofectamine 3000 reagent (Invitrogen) was used for transfection for 5 hours, and media were replaced with DMEM (Gibco) with 10% fetal bovine serum for the next 48 hours. Cells were subsequently collected, and luciferase reporter assay was performed with the Firefly and Renilla Single Tube Luciferase Assay Kit (Biotium) following the manufacturer's provided protocol. Firefly and renilla luminescence were measured by Infinite M Plex (Tecan) plate reader. Firefly luciferase luminescence activity was normalized by Renilla luciferase luminescence to control for differences in cell number/well.

FGF21 measurements—Rodent plasma Fgf21 measurements were performed using Rat/Mouse ELISA kit from Sigma Aldrich (catalogue number-EZRMFGF21-26K; Lot number 3280681). Human FGF21 measurements were performed using an FGF-21 ELISA Kit from Millipore Sigma (catalogue number-EZHFGF21-19K).

Triglyceride estimation in liver tissue—Lipids were extracted from 10–20 mg of liver tissue following a prior published protocol[75] with some modifications. Briefly, 225 μl of ice-cold methanol was added to the ground liver tissue, homogenized, and 750 μl methyl tert-butyl ether (MTBE) was added. The sample was vortexed for 20 mins, and 188 μl of distilled water was added and centrifuged for 2 minutes at 14,000 × *g*. 700 μl of the upper organic phase was transferred into a new tube and dried in a vacuum centrifuge (Vacufuge plus, Eppendorf). Extracted lipids were dissolved in 100 μl of ethanol containing 1% Triton X-100 (Sigma-Aldrich). The triglyceride concentration in extracted lipids was measured using a triglyceride-SL assay kit (Sekisui, Cat no. 236–60) and normalized to liver tissue weight.

Western Blotting—HEK293T cells transfected with pcDNA3.1-eGFP (negative control) or pcDNA3.1-ChREBPα were resuspended in radioimmunoprecipitation assay (RIPA) buffer (Boston BioProducts) supplemented with Protease and Phosphatase Inhibitor Cocktail (Cell Signaling). The cells were incubated on ice for 30 min with intermittent vortexing. Lysates were then centrifuged at 16,000 RCF and 4 °C for 20 minutes, and the supernatant was stored at −80 °C until further use. Transferred polyvinylidene fluoride membranes were blocked in 5% skim milk in 1X TBST for 1 hour. Primary antibodies (ChREBP 1:1,000, Novusb Biologicals and β-Actin 1: 1,000, Cell Signaling) were added and the membranes were incubated overnight. Subsequently, the membranes were blotted with an anti-rabbit IgG-HRP secondary antibody (1:10,000, Invitrogen) and developed with a chemiluminescent substrate (Western Lightning Plus-ECL, PerkinElmer).

GSEA Analyses of human liver and organoid RNAseq data sets—GSEA[39,76] was performed using GSEA software version 4.2.2 (http://software.broadinstitute.org/gsea/). We analyzed GEO data sets GSE130970[41], GSE135251[32], GSE48452[43], GSE83452[77], dbGAP database phs001807[78], and EBI databases E-MTAB-11688[42], which contain RNAseq or microarray data of patients with and without hepatic steatosis and/or before or after bariatric surgery, and GSE213932 for human liver organoids derived from patients with different *GCKR* genotypes. Genes in each dataset were pre-ranked using the formula Rank = $-\log_{10}(P)*(sign(log_2(fold\ changes)))$. For Figure 5, samples with TT versus CC genotypes were compared, which for GSE135251 was determined by FASTQ reads across rs1260326. For Figure 7 we compared samples with hepatic steatosis versus non-steatotic controls when this data was available (GSE130970, dbGAPphs001807, GSE13521, GSE48452, E-MTAB-11688), or pre and post bariatric surgery when steatosis information was not available (GSE83452) as indicated, with *P* calculated using Student's t test (paired for when paired biopsies were available, unpaired otherwise). GSEA was performed on these pre ranked gene lists using the 160 NADH-responsive genes derived from the RNAseq experiments in Figure 1 (Supplementary Table 1).

Trait analysis from *GCKR*, ChREBP, and *FGF21* variants—For Fig 6I, phenotypes associated with either *GCKR*, *MLXIPL*, or *FGF21* were downloaded from the Type 2 Diabetes Knowledge Portal[36]. Significant traits were defined as a p-value of < 2.5E-6 calculated using the MAGMA (Multi-marker analysis of Genomic Annotation) method, which is a generally accepted threshold for significance of MAGMA results.

Mass spectrometry measurements—α-hydroxybutyrate levels for the *Lb*NOX/ethanol and ethanol/fomepizole *in vivo* experiments (Figure 1C *Lb*NOX/Ethanol measurements, Figure S1B and Figure S1E) measured on an LC-MS as previously described[1], and the Figure 1C *Lb*NOX/Ethanol measurements and S1B measurements were previously reported [1].

For intracellular metabolite measurements of 293T cells (Figure 4), metabolomics was performed through the Metabolomics Platform at the Comprehensive Cancer Center at the University of Chicago. 48 hours after transfection with the specified plasmid, cells were washed with room-temperature PBS, immediately quenched with dry-ice-cold 80% methanol, and transferred to conical tubes. Samples were centrifuged at 20,000 g for 20

minutes at 4°C, the supernatant was dried down on a Genvevac EZ-2 4.0 elite evaporator, and the samples were resuspended in 100 uL of 60/40 acetonitrile-water. Metabolite separation was performed using Thermo Scientific Vanquish Horizon UHPLC system and iHILIC-(P) Classic (2.1×150 mm, 5 μm; part # 160.152.0520; HILICON AB) column. MS detection was done using an Orbitrap IQ-X Tribrid mass spectrometer (Thermo Scientific) with a H-ESI probe operating in switch polarity. The mobile phase A (MPA) was 20 mM ammonium bicarbonate at pH 9.6, adjusted by ammonium hydroxide addition and mobile phase B (MPB) was acetonitrile. The column temperature, injection volume, and the flow rate were 40°C, 2 μL, and 0.2mL/minute, respectively. The chromatographic gradient was 0 minutes: 85% B, 0.5 minutes: 85% B, 18 minutes: 20% B, 20 minutes: 20% B, 20.5 minutes: 85% B and 28 minutes: 85% B. MS parameters were as follows: Acquisition range of 70–1000 m/z at 60K resolution, spray voltage:3600V for positive ionization and 2800 for negative ionization modes, sheath gas: 35, auxiliary gas: 5, sweep gas: 1, ion transfer tube temperature: 250°C, vaporizer temperature: 350°C, AGC target: 100%, and a maximum injection time of 118 ms. AcquireX workflow was used to collect the MS/MS data in negative and positive separately using the assisted HCD collision energy 20,35,50,75,100 as well as targeted MS/MS with a defined retention time window for the in-house retention time database. Data acquisition was done using the Xcalibur software (Thermo Scientific) and data analysis was performed using Compound Discoverer 3.3 & Tracefinder 5.1 software (Thermo Scientific). Metabolite identification was done by matching the retention time and MS/MS fragmentation to the in-house database generated using the reference standards. In the data table, the “RT+MS/MS” indicates the matching retention time & MS/MS, “RT”-indicates the only matching retention time and doesn’t have MS/MS while the MS/MS is for carnitine species identified based on the 85.02841+/5 ppm fragment.

For sugar phosphate measurements, cells were washed with 1 mL room temperature normal saline, which was immediately aspirated, at which point 1 mL −20°C chilled 80% methanol containing 0.1 μg/ml [$^{13}C_3$] glyceraldehyde3P was added. Cells were scraped and then centrifuged at 15000 × g at 4°C for 5 min. Five-hundred microliters of supernatant were dried in a vacuum centrifuge and then derivatized per the method described in Okahashi et. al. (2019; PMID: 30176394) with slight modifications[79]. To the dried extract 50 μl of 20 mg/ml of o-(2,3,4,5,6-pentafluorobenzyl) hydroxylamine hydrochloride in pyridine was added, followed by incubation at 60°C for 1h. The pentafluorobenzyl oxime derivatives were further derivatized by adding 50 μl of MSTFA+1% TMCS and incubating at 60°C for 30 min. The samples were then briefly centrifuged at 15000 × g for 1 min and then packed in glass vials for measurement. Samples were measured in the negative mode of chemical ionization with methane as reagent gas and helium as carrier gas. One microliter of sample was injected into the 8890 GC connected to a DB-1 MS column (30 m × 0.25 mm × 0.25 μm) with 10m duraguard column coupled to 5977B mass spectrometer. The inlet temperature was set to 250°C, and helium flow was set to 13.071 psi with a septum purge flow of 3 ml/min. Samples were measured with a split ratio of 10:1. The column was set to 60°C for 2 min, then to 20°C/min to a temperature of 200°C, followed by 5°C/min to a final temperature of 260°C, this was followed by 2°C/min to a final temperature of 275°C, and then 20°C/min to a final temperature of 325°C and held for 2 min. A constant flow of 1.1ml/min was applied to separate the compounds on the column. A solvent delay of

11 min was applied. Samples were measured in SIM mode in negative chemical ionization mode. SIM ions used were 400 for unlabeled glyceraldehyde-3 phosphate, 403 for $^{13}C_3$ glyceraldehyde-3 phosphate, 604 for all pentose and pentulose 5 phosphates, 706 for hexose 6 phosphates, 544 for fructose1,6 bisphosphates. Retention times and ions were confirmed by running authentic standards for all the metabolites. A gain factor of 3x was applied for hexose phosphates and a gain factor of 5 was applied for fructose 1,6 bisphosphate. The remaining metabolite measurements were analyzed on a GC-MS as previously described[80]. 20 μL samples (media or plasma) were combined with 160 μL of methanol precooled to −80°C. 20 μL of 2 mM tricarballylic acid was added to this as an internal standard. Samples were then vortexed and incubated at −80°C for 10 min followed by centrifugation at 13000 × g for 5 min at 4°C. Samples were dried in a vacuum centrifuge, derivatized as previously reported[81], and analyzed on a 8890 GC coupled to EI/CI 5977B mass selective detector mass spectrometer (Agilent) using an electron impact ionization extractor ion source. One μL of the sample was injected in split mode with 1:5 (split 5) of the sample entering the mass spectrometer. Full scan data was recorded with a scan window of 50 to 800 m/z. The front inlet heater was set to 250 °C with a septum purge flow of 3 mL/min. Samples were injected onto a DB-5ms dura guard inert 40 m × 250 μm × 0.25 μm column connected to MSD. Samples were measured in a constant flow mode with a helium flow rate set at 1.1 mL/min. The starting temperature of the oven was set at 60 °C for 1 min and then ramped at 10 °C/min to 325 °C to separate analytes, with a final hold time of 10 min.

For Figure 4, certain metabolites (e.g. Glyceradehyde-3-phosphate) were measured in both LC-MS and GC-MS methods in separate experiments and in such cases, we reported the highest correlation for such metabolites.

QUANTIFICATION AND STATISTICAL ANALYSIS

Data are reported as mean +/− SEM. Sample size is indicated in Figures with each individual data point representing an experimental replicate. Unless otherwise described below statistical analyses were performed using R version 4.2.2. *P* and adjusted *P* values for RNAseq data were calculated using DESeq2 version 1.38.3, which uses the Wald test for *P* calculations with Benjamini-Hochberg procedure for adjusted *P* value calculations. Students T-tests were used for analysis of individual RNAseq and QPCR transcript abundance, luciferase reporter assays, lipid measurements, L/P levels, FGF21, and mouse plasma αHB and acetate abundance. For traits that were previously linked to *GCKR* genetic variation in a specific direction (e.g. an increase in FGF21), one-tailed Student's *t* tests were used; otherwise two-tailed Student's *t* test were used. The correlation of intracellular metabolite abundance to luciferase activity was calculated using Pearson's correlation coefficient. One way ANOVA was used for analysis of luciferase abundance over increasing glucose concentration. The significance of overlapping gene sets was calculated using Chi-square analysis. Welch's T-tests were used for analysis of Human αHB, serum FGF21, and serum triglycerides.

Supplementary Material

Refer to Web version on PubMed Central for supplementary material.

ACKNOWLEDGEMENTS

R.P.G. was supported the US National Institutes of Health (NIH) grants K08DK1158811, R03DK131243, and R01DK134675, a Pinnacle Research Award from the American Association for the Study of Liver Disease (AASLD), and a Burroughs-Wellcome Career Award for Medical Scientists (CAMS). V.C. was supported by NIH grants K99GM121856, R35GM142495, R03AG067301, and Longevity Impetus Grants. V.K.M. is an Investigator of the Howard Hughes Medical Institute and was additionally supported by NIH grant R35GM122455 and the Marriott Foundation. We thank the Harvard University Biopolymers Facility for assistance with RNA sequencing, and the University of Chicago Medicine Comprehensive Cancer Center for assistance with metabolomics measurements (RRID:SCR_022932).

REFERENCES

1. Goodman RP, Markhard AL, Shah H, Sharma R, Skinner OS, Clish CB, Deik A, Patgiri A, Hsu Y-HH, Masia R, et al. (2020). Hepatic NADH reductive stress underlies common variation in metabolic traits. Nature. 10.1038/s41586-020-2337-2.
2. van SCHAFTINGEN E (1989). A protein from rat liver confers to glucokinase the property of being antagonistically regulated by fructose 6-phosphate and fructose 1-phosphate. Eur J Biochem 179, 179–184. 10.1111/j.1432-1033.1989.tb14538.x. [PubMed: 2917560]
3. Hale C, Lloyd DJ, Pellacani A, and Véniant MM (2015). Molecular targeting of the GK-GKRP pathway in diabetes. Expert Opin Ther Targets 19, 129–139. 10.1517/14728222.2014.965681. [PubMed: 25324018]
4. Diabetes Genetics Initiative of Broad Institute of Harvard and MIT, Lund University, and N.I. of B.R., Saxena R, Voight BF, Lyssenko V, Burtt NP, de Bakker PIW, Chen H, Roix JJ, Kathiresan S, Hirschhorn JN, et al. (2007). Genome-wide association analysis identifies loci for type 2 diabetes and triglyceride levels. Science 316, 1331–1336. 10.1126/science.1142358. [PubMed: 17463246]
5. Beer NL, Tribble ND, McCulloch LJ, Roos C, Johnson PRV, Orho-Melander M, and Gloyn AL (2009). The P446L variant in GCKR associated with fasting plasma glucose and triglyceride levels exerts its effect through increased glucokinase activity in liver. Hum Mol Genet 18, 4081–4088. 10.1093/hmg/ddp357. [PubMed: 19643913]
6. Speliotes EK, Yerges-Armstrong LM, Wu J, Hernaez R, Kim LJ, Palmer CD, Gudnason V, Eiriksdottir G, Garcia ME, Launer LJ, et al. (2011). Genome-wide association analysis identifies variants associated with nonalcoholic fatty liver disease that have distinct effects on metabolic traits. PLoS Genet 7, e1001324. 10.1371/journal.pgen.1001324. [PubMed: 21423719]
7. Wang J, Liu S, Wang B, Miao Z, Han L, Chu N, Zhang K, Meng D, Li C, and Ma X (2012). Association between gout and polymorphisms in GCKR in male Han Chinese. Hum Genet 131, 1261–1265. 10.1007/s00439-012-1151-9. [PubMed: 22395765]
8. Cheung CYY, Tang CS, Xu A, Lee C-H, Au K-W, Xu L, Fong CHY, Kwok KHM, Chow W-S, Woo Y-C, et al. (2017). An Exome-Chip Association Analysis in Chinese Subjects Reveals a Functional Missense Variant of *GCKR* That Regulates FGF21 Levels. Diabetes 66, 1723–1728. 10.2337/db16-1384. [PubMed: 28385800]
9. Cornelis MC, Byrne EM, Esko T, Nalls MA, Ganna A, Paynter N, Monda KL, Amin N, Fischer K, Renstrom F, et al. (2015). Genome-wide meta-analysis identifies six novel loci associated with habitual coffee consumption. Mol Psychiatry 20, 647–656. 10.1038/mp.2014.107. [PubMed: 25288136]
10. Schumann G, Liu C, O'Reilly P, Gao H, Song P, Xu B, Ruggeri B, Amin N, Jia T, Preis S, et al. (2016). KLB is associated with alcohol drinking, and its gene product β-Klotho is necessary for FGF21 regulation of alcohol preference. Proc Natl Acad Sci U S A 113, 14372–14377. 10.1073/pnas.1611243113. [PubMed: 27911795]
11. Yamashita H, Takenoshita M, Sakurai M, Bruick RK, Henzel WJ, Shillinglaw W, Arnot D, and Uyeda K (2001). A glucose-responsive transcription factor that regulates carbohydrate metabolism in the liver. Proc Natl Acad Sci U S A 98, 9116–9121. 10.1073/pnas.161284298. [PubMed: 11470916]
12. Iizuka K, Bruick RK, Liang G, Horton JD, and Uyeda K (2004). Deficiency of carbohydrate response element-binding protein (ChREBP) reduces lipogenesis as well as glycolysis. Proc Natl Acad Sci U S A 101, 7281–7286. 10.1073/pnas.0401516101. [PubMed: 15118080]

13. Kim M, Lai M, Herman MA, Kim M, Krawczyk SA, Doridot L, Fowler AJ, Wang JX, Trauger SA, Noh H, et al. (2016). ChREBP regulates fructose-induced glucose production independently of insulin signaling. Journal of Clinical Investigation 126, 4372–4386. 10.1172/JCI81993.tor. [PubMed: 27669460]
14. Liangpunsakul S, Ross RA, and Crabb DW (2013). Activation of carbohydrate response element-binding protein by ethanol. Journal of Investigative Medicine 61, 270–277. 10.2310/JIM.0b013e31827c2795. [PubMed: 23266705]
15. Titov DV, Cracan V, Goodman RP, Peng J, Grabarek Z, and Mootha VK (2016). Complementation of mitochondrial electron transport chain by manipulation of the NAD+/NADH ratio. Science 352, 231–235. 10.1126/science.aad4017. [PubMed: 27124460]
16. Heacock ML, Abdulaziz EN, Pan X, Zuckerman AL, Violante S, Yao C, Cross JR, and Cracan V (2022). A genetically encoded tool to increase cellular NADH/NAD+ ratio in living cells. bioRxiv, 2022.09.20.508785. 10.1101/2022.09.20.508785.
17. Geng L, Lam KSL, and Xu A (2020). The therapeutic potential of FGF21 in metabolic diseases: from bench to clinic. Nat Rev Endocrinol 16, 654–667. 10.1038/s41574-020-0386-0. [PubMed: 32764725]
18. Romeo S, Kozlitina J, Xing C, Pertsemlidis A, Cox D, Pennacchio LA, Boerwinkle E, Cohen JC, and Hobbs HH (2008). Genetic variation in PNPLA3 confers susceptibility to nonalcoholic fatty liver disease. Nat Genet 40, 1461–1465. 10.1038/ng.257. [PubMed: 18820647]
19. Liao Y, Wang J, Jaehnig EJ, Shi Z, and Zhang B (2019). WebGestalt 2019: gene set analysis toolkit with revamped UIs and APIs. Nucleic Acids Res 47, W199–W205. 10.1093/nar/gkz401. [PubMed: 31114916]
20. Abdul-Wahed A, Guilmeau S, and Postic C (2017). Sweet Sixteenth for ChREBP: Established Roles and Future Goals. Cell Metab 26, 324–341. 10.1016/j.cmet.2017.07.004. [PubMed: 28768172]
21. Iizuka K, Miller B, and Uyeda K (2006). Deficiency of carbohydrate-activated transcription factor ChREBP prevents obesity and improves plasma glucose control in leptin-deficient (ob/ob) mice. Am J Physiol Endocrinol Metab 291, 358–364. 10.1152/ajpendo.00027.2006.
22. Keenan AB, Torre D, Lachmann A, Leong AK, Wojciechowicz ML, Utti V, Jagodnik KM, Kropiwnicki E, Wang Z, and Ma'ayan A (2019). ChEA3: transcription factor enrichment analysis by orthogonal omics integration. Nucleic Acids Res 47, W212–W224. 10.1093/nar/gkz446. [PubMed: 31114921]
23. Krebs HA (1967). The redox state of nicotinamide adenine dinucleotide in the cytoplasm and mitochondria of rat liver. Adv Enzyme Regul 5, 409–434. 10.1016/0065-2571(67)90029-5. [PubMed: 4301794]
24. Kabashima T, Kawaguchi T, Wadzinski BE, and Uyeda K (2003). Xylulose 5-phosphate mediates glucose-induced lipogenesis by xylulose 5-phosphate-activated protein phosphatase in rat liver. Proc Natl Acad Sci U S A 100, 5107–5112. 10.1073/pnas.0730817100. [PubMed: 12684532]
25. Dentin R, Tomas-Cobos L, Foufelle F, Leopold J, Girard J, Postic C, and Ferré P (2012). Glucose 6-phosphate, rather than xylulose 5-phosphate, is required for the activation of ChREBP in response to glucose in the liver. J Hepatol 56, 199–209. 10.1016/j.jhep.2011.07.019. [PubMed: 21835137]
26. Li MV, Chen W, Harmancey RN, Nuotio-Antar AM, Imamura M, Saha P, Taegtmeyer H, and Chan L (2010). Glucose-6-phosphate mediates activation of the carbohydrate responsive binding protein (ChREBP). Biochem Biophys Res Commun 395, 395–400. 10.1016/j.bbrc.2010.04.028. [PubMed: 20382127]
27. Arden C, Tudhope SJ, Petrie JL, Al-Oanzi ZH, Cullen KS, Lange AJ, Towle HC, and Agius L (2012). Fructose 2,6-bisphosphate is essential for glucose-regulated gene transcription of glucose-6-phosphatase and other ChREBP target genes in hepatocytes. Biochemical Journal 443, 111–123. 10.1042/bj20111280. [PubMed: 22214556]
28. Agius L, Chachra SS, and Ford BE (2020). The Protective Role of the Carbohydrate Response Element Binding Protein in the Liver: The Metabolite Perspective. Front Endocrinol (Lausanne) 11, 1–10. 10.3389/fendo.2020.594041. [PubMed: 32038495]

29. Rhee EP, Ho JE, Chen M-H, Shen D, Cheng S, Larson MG, Ghorbani A, Shi X, Helenius IT, O'Donnell CJ, et al. (2013). A genome-wide association study of the human metabolome in a community-based cohort. Cell Metab 18, 130–143. 10.1016/j.cmet.2013.06.013. [PubMed: 23823483]
30. Leite SB, Roosens T, El Taghdouini A, Mannaerts I, Smout AJ, Najimi M, Sokal E, Noor F, Chesne C, and van Grunsven LA (2016). Novel human hepatic organoid model enables testing of drug-induced liver fibrosis in vitro. Biomaterials 78, 1–10. 10.1016/J.BIOMATERIALS.2015.11.026. [PubMed: 26618472]
31. Cuykx M, Claes L, Rodrigues RM, Vanhaecke T, and Covaci A (2018). Metabolomics profiling of steatosis progression in HepaRG® cells using sodium valproate. Toxicol Lett 286, 22–30. 10.1016/J.TOXLET.2017.12.015. [PubMed: 29355688]
32. Govaere O, Cockell S, Tiniakos D, Queen R, Younes R, Vacca M, Alexander L, Ravaioli F, Palmer J, Petta S, et al. (2020). Transcriptomic profiling across the nonalcoholic fatty liver disease spectrum reveals gene signatures for steatohepatitis and fibrosis. Sci Transl Med 12, 1–18. 10.1126/SCITRANSLMED.ABA4448.
33. Kimura M, Iguchi T, Iwasawa K, Dunn A, Thompson WL, Yoneyama Y, Chaturvedi P, Zorn AM, Wintzinger M, Quattrocelli M, et al. (2022). En masse organoid phenotyping informs metabolic-associated genetic susceptibility to NASH. Cell 185, 4216–4232.e16. 10.1016/j.cell.2022.09.031. [PubMed: 36240780]
34. Kim W, Deik A, Gonzalez C, Gonzalez ME, Fu F, Ferrari M, Churchhouse CL, Florez JC, Jacobs SBR, Clish CB, et al. Polyunsaturated Fatty Acid Desaturation Is a Mechanism for Glycolytic NAD+ Recycling. Preprint, 10.1016/J.CMET.2018.12.023 10.1016/J.CMET.2018.12.023.
35. Fernandes Silva L, Vangipurapu J, Kuulasmaa T, and Laakso M (2019). An intronic variant in the GCKR gene is associated with multiple lipids. Sci Rep 9, 10240. 10.1038/s41598-019-46750-3. [PubMed: 31308433]
36. Costanzo MC, von Grotthuss M, Massung J, Jang D, Caulkins L, Koesterer R, Gilbert C, Welch RP, Kudtarkar P, Hoang Q, et al. (2023). The Type 2 Diabetes Knowledge Portal: An open access genetic resource dedicated to type 2 diabetes and related traits. Cell Metab 35, 695–710.e6. 10.1016/j.cmet.2023.03.001. [PubMed: 36963395]
37. Jang C, Hui S, Zeng X, Cowan AJ, Wang L, Chen L, Morscher RJ, Reyes J, Frezza C, Hwang HY, et al. (2019). Metabolite Exchange between Mammalian Organs Quantified in Pigs. Cell Metab, 1–13. 10.1016/j.cmet.2019.06.002.
38. Yilmaz Y, Eren F, Yonal O, Kurt R, Aktas B, Celikel CA, Ozdogan O, Imeryuz N, Kalayci C, and Avsar E (2010). Increased serum FGF21 levels in patients with nonalcoholic fatty liver disease. Eur J Clin Invest 40, 887–892. 10.1111/j.1365-2362.2010.02338.x. [PubMed: 20624171]
39. Subramanian A, Tamayo P, Mootha VK, Mukherjee S, Ebert BL, Gillette MA, Paulovich A, Pomeroy SL, Golub TR, Lander ES, et al. (2005). Gene set enrichment analysis: a knowledge-based approach for interpreting genome-wide expression profiles. Proc Natl Acad Sci U S A 102, 15545–15550. 10.1073/pnas.0506580102. [PubMed: 16199517]
40. Spiegelman B, Ridderstråle M, Puigserver P, Eriksson K-F, Lander ES, Laurila E, Altshuler D, Mootha VK, Subramanian A, Lehar J, et al. (2003). PGC-1α-responsive genes involved in oxidative phosphorylation are coordinately downregulated in human diabetes. Nat Genet 34, 267–273. [PubMed: 12808457]
41. Hoang SA, Oseini A, Feaver RE, Cole BK, Asgharpour A, Vincent R, Siddiqui M, Lawson MJ, Day NC, Taylor JM, et al. (2019). Gene Expression Predicts Histological Severity and Reveals Distinct Molecular Profiles of Nonalcoholic Fatty Liver Disease. Sci Rep 9, 1–14. 10.1038/s41598-019-48746-5. [PubMed: 30626917]
42. Pellegrina D, Prayitno K, Azhie A, Pasini E, Baciu C, Fischer S, Reimand J, and Bhat M (2023). Transcriptomic changes in liver transplant recipients with non-alcoholic steatohepatitis indicate dysregulation of wound healing. Front Endocrinol (Lausanne) 14, 1–10. 10.3389/fendo.2023.1111614.
43. Ahrens M, Ammerpohl O, Von Schönfels W, Kolarova J, Bens S, Itzel T, Teufel A, Herrmann A, Brosch M, Hinrichsen H, et al. (2013). DNA methylation analysis in nonalcoholic fatty liver disease suggests distinct disease-specific and remodeling signatures after bariatric surgery. Cell Metab 18, 296–302. 10.1016/j.cmet.2013.07.004. [PubMed: 23931760]

44. Shantavasinkul PC, Muehlbauer MJ, Bain JR, Ilkayeva OR, Craig DM, Newgard CB, Svetkey LP, Shah SH, and Torquati A (2018). Improvement in insulin resistance after gastric bypass surgery is correlated with a decline in plasma 2-hydroxybutyric acid. Surgery for Obesity and Related Diseases 14, 1126–1132. 10.1016/j.soard.2018.03.033. [PubMed: 29805089]
45. Mummadi RR, Kasturi KS, Chennareddygari S, and Sood GK (2008). Effect of Bariatric Surgery on Nonalcoholic Fatty Liver Disease: Systematic Review and Meta-Analysis. Clinical Gastroenterology and Hepatology 6, 1396–1402. 10.1016/j.cgh.2008.08.012. [PubMed: 18986848]
46. Landaas S, and Pettersen JE (1975). Clinical conditions associated with urinary excretion of 2-hydroxybutyric acid. Scand J Clin Lab Invest 35, 259–266. 10.1080/00365517509095738. [PubMed: 168632]
47. Goodman RP, Calvo SE, and Mootha VK (2018). Spatiotemporal compartmentalization of hepatic NADH and NADPH metabolism. Journal of Biological Chemistry 293, 7508–7516. 10.1074/jbc.TM117.000258. [PubMed: 29514978]
48. Burgess SC, Iizuka K, Nam HJ, Harris RA, Kashiwaya Y, Veech RL, Kitazume T, and Uyeda K (2008). Carbohydrate-response element-binding protein deletion alters substrate utilization producing an energy-deficient liver. Journal of Biological Chemistry 283, 1670–1678. 10.1074/jbc.M706540200. [PubMed: 18042547]
49. Raimondo A, Rees MG, and Gloyn AL (2015). Glucokinase regulatory protein: Complexity at the crossroads of triglyceride and glucose metabolism. Curr Opin Lipidol 26, 88–95. 10.1097/MOL.0000000000000155. [PubMed: 25692341]
50. Machiela MJ, and Chanock SJ (2015). LDlink: A web-based application for exploring population-specific haplotype structure and linking correlated alleles of possible functional variants. Bioinformatics 31, 3555–3557. 10.1093/bioinformatics/btv402. [PubMed: 26139635]
51. Iizuka K, Takeda J, and Horikawa Y (2009). Glucose induces FGF21 mRNA expression through ChREBP activation in rat hepatocytes. FEBS Lett 583, 2882–2886. 10.1016/j.febslet.2009.07.053. [PubMed: 19660458]
52. Pazoki R, Evangelou E, Mosen-Ansorena D, Pinto RC, Karaman I, Blakeley P, Gill D, Zuber V, Elliott P, Tzoulaki I, et al. (2019). GWAS for urinary sodium and potassium excretion highlights pathways shared with cardiovascular traits. Nat Commun 10. 10.1038/s41467-019-11451-y.
53. Köttgen A, Pattaro C, Böger CA, Fuchsberger C, Olden M, Glazer NL, Parsa A, Gao X, Yang Q, Smith AV, et al. (2010). New loci associated with kidney function and chronic kidney disease. Nat Genet 42, 376–384. 10.1038/ng.568. [PubMed: 20383146]
54. Giontella A, Zagkos L, Geybels M, Larsson SC, Tzoulaki I, Mantzoros CS, Andersen B, Gill D, and Cronj T (2023). Renoprotective effects of genetically proxied fibroblast growth factor 21 : Mendelian randomization, proteome-wide and metabolome-wide association study. 145. 10.1016/j.metabol.2023.155616.
55. Flippo KH, Trammell SAJ, Gillum MP, Aklan I, Perez MB, Yavuz Y, Smith NK, Jensen-Cody SO, Zhou B, Claflin KE, et al. (2022). FGF21 suppresses alcohol consumption through an amygdalo-striatal circuit. Cell Metab 34, 317–328.e6. 10.1016/j.cmet.2021.12.024. [PubMed: 35108517]
56. Younossi ZM, Stepanova M, Afendy M, Fang Y, Younossi Y, Mir H, and Srishord M (2011). Changes in the Prevalence of the Most Common Causes of Chronic Liver Diseases in the United States From 1988 to 2008. Clinical Gastroenterology and Hepatology 9, 524–530.e1. 10.1016/j.cgh.2011.03.020. [PubMed: 21440669]
57. Parrish NF, Feurer ID, Matsuoka LK, Rega SA, Perri R, and Alexopoulos SP (2019). The Changing Face of Liver Transplantation in the United States: The Effect of HCV Antiviral Eras on Transplantation Trends and Outcomes. Transplant Direct 5, 1–7. 10.1097/TXD.0000000000000866. [PubMed: 30882030]
58. Wagner-Skacel J, Horvath A, Grande P, Wenninger J, Matzer F, Fazekas C, Mörkl S, Meinitzer A, and Stadlbauer V (2021). Association of fibroblast growth factor 21 with alcohol consumption and alcohol liver cirrhosis. Neuropsychiatrie 35, 140–146. 10.1007/s40211-020-00380-8. [PubMed: 33330965]
59. Williams Amy AL, Jacobs Suzanne SBR, Moreno-Macías H, Huerta-Chagoya A, Churchhouse C, Márquez-Luna C, Gómez-Vázquez MJ, Burtt Noël NP, Aguilar-Salinas CA, González-Villalpando C, et al. (2014). Sequence variants in SLC16A11 are a common risk factor for type 2 diabetes in Mexico. Nature 506, 97. 10.1038/NATURE12828. [PubMed: 24390345]

60. Kim W, Deik A, Gonzalez C, Gonzalez ME, Fu F, Ferrari M, Churchhouse CL, Florez JC, Jacobs SBR, Clish CB, et al. (2019). Polyunsaturated Fatty Acid Desaturation Is a Mechanism for Glycolytic NAD+ Recycling. Cell Metab 0, 1–15. 10.1016/J.CMET.2018.12.023.

61. Dentin R, Benhamed F, Hainault I, Fauveau V, Foufelle F, Dyck JRB, Girard J, and Postic C (2006). Liver-Specific Inhibition of ChREBP Improves Hepatic Steatosis and Insulin Resistance in ob/ob Mice. Diabetes 55, 2159–2170. 10.2337/DB06-0200. [PubMed: 16873678]

62. Guan D, and Lazar MA (2022). Circadian Regulation of Gene Expression and Metabolism in the Liver. Semin Liver Dis 42, 113–121. 10.1055/a-1792-4240. [PubMed: 35263797]

63. Ramsey KM, Yoshino J, Brace CS, Abrassart D, Kobayashi Y, Marcheva B, Hong H, Chong JL, Buhr ED, Lee C, et al. (2009). Circadian clock feedback cycle through NAMPT-mediated NAD+ biosynthesis. Science 324, 651–654. 10.1126/science.1171641. [PubMed: 19299583]

64. Arden C, Petrie JL, Tudhope SJ, Al-Oanzi Z, Claydon AJ, Beynon RJ, Towle HC, and Agius L (2011). Elevated glucose represses liver glucokinase and induces its regulatory protein to safeguard hepatic phosphate homeostasis. Diabetes 60, 3110–3120. 10.2337/db11-0061. [PubMed: 22013014]

65. Ronchi JA, Figueira TR, Ravagnani FG, Oliveira HCF, Vercesi AE, and Castilho RF (2013). A spontaneous mutation in the nicotinamide nucleotide transhydrogenase gene of C57BL/6J mice results in mitochondrial redox abnormalities. Free Radic Biol Med 63, 446–456. 10.1016/j.freeradbiomed.2013.05.049. [PubMed: 23747984]

66. Aguilar-Arnal L, Ranjit S, Stringari C, Orozco-Solis R, Gratton E, and Sassone-Corsi P (2016). Spatial dynamics of SIRT1 and the subnuclear distribution of NADH species. Proceedings of the National Academy of Sciences 113, 12715–12720. 10.1073/pnas.1609227113.

67. Levine DC, Kuo HY, Hong HK, Cedernaes J, Hepler C, Wright AG, Sommars MA, Kobayashi Y, Marcheva B, Gao P, et al. (2021). NADH inhibition of SIRT1 links energy state to transcription during time-restricted feeding. Nat Metab 3, 1621–1632. 10.1038/s42255-021-00498-1. [PubMed: 34903884]

68. Zhang Q, Piston DW, and Goodman RH (2002). Regulation of corepressor function by nuclear NADH. Science (1979) 295, 1895–1897. 10.1126/science.1069300.

69. Rhee EP, Yang Q, Yu B, Liu X, Cheng S, Deik A, Pierce KA, Bullock K, Ho JE, Levy D, et al. (2016). An exome array study of the plasma metabolome. Nat Commun 7, 1–7. 10.1038/ncomms12360.

70. Corey KE, Pitts R, Lai M, Loureiro J, Masia R, Osganian SA, Gustafson JL, Hutter MM, Gee DW, Meireles OR, et al. (2022). ADAMTSL2 protein and a soluble biomarker signature identify at-risk non-alcoholic steatohepatitis and fibrosis in adults with NAFLD. J Hepatol 76, 25–33. 10.1016/j.jhep.2021.09.026. [PubMed: 34600973]

71. Patro R, Duggal G, Love MI, Irizarry RA, and Kingsford C (2017). Salmon provides fast and bias-aware quantification of transcript expression. Nat Methods 14, 417–419. 10.1038/nmeth.4197. [PubMed: 28263959]

72. Love MI, Huber W, and Anders S (2014). Moderated estimation of fold change and dispersion for RNA-seq data with DESeq2. Genome Biol 15, 1–21. 10.1186/s13059-014-0550-8.

73. Liao Y, Wang J, Jaehnig EJ, Shi Z, and Zhang B (2019). WebGestalt 2019: gene set analysis toolkit with revamped UIs and APIs. Nucleic Acids Res 47, W199–W205. 10.1093/nar/gkz401. [PubMed: 31114916]

74. Lou DQ, Tannour M, Selig L, Thomas D, Kahn A, and Vasseur-Cogne M (1999). Chicken ovalbumin upstream promoter-transcription factor II, a new partner of the glucose response element of the L-type pyruvate kinase gene, acts as an inhibitor of the glucose response. Journal of Biological Chemistry 274, 28385–28394. 10.1074/jbc.274.40.28385. [PubMed: 10497199]

75. Cajka T, Smilowitz JT, and Fiehn O (2017). Validating Quantitative Untargeted Lipidomics Across Nine Liquid Chromatography-High-Resolution Mass Spectrometry Platforms. Anal Chem 89, 12360–12368. 10.1021/acs.analchem.7b03404. [PubMed: 29064229]

76. Mootha VK, Lindgren CM, Eriksson K-F, Subramanian A, Sihag S, Lehar J, Puigserver P, Carlsson E, Ridderstråle M, Laurila E, et al. (2003). PGC-1alpha-responsive genes involved in oxidative phosphorylation are coordinately downregulated in human diabetes. Nat Genet 34, 267–273. 10.1038/ng1180. [PubMed: 12808457]

77. Haas JT, Vonghia L, Mogilenko DA, Verrijken A, Molendi-Coste O, Fleury S, Deprince A, Nikitin A, Woitrain E, Ducrocq-Geoffroy L, et al. (2019). Transcriptional network analysis implicates altered hepatic immune function in NASH development and resolution. Nat Metab 1, 604–614. 10.1038/s42255-019-0076-1. [PubMed: 31701087]

78. Argemi J, Latasa MU, Atkinson SR, Blokhin IO, Massey V, Gue JP, Cabezas J, Lozano JJ, Van Booven D, Bell A, et al. (2019). Defective HNF4alpha-dependent gene expression as a driver of hepatocellular failure in alcoholic hepatitis. Nat Commun 10. 10.1038/s41467-019-11004-3.

79. Okahashi N, Maeda K, Kawana S, Iida J, Shimizu H, and Matsuda F (2019). Sugar phosphate analysis with baseline separation and soft ionization by gas chromatography-negative chemical ionization-mass spectrometry improves flux estimation of bidirectional reactions in cancer cells. Metab Eng 51, 43–49. 10.1016/j.ymben.2018.08.011. [PubMed: 30176394]

80. Singh C, Hoppe G, Tran V, McCollum L, Bolok Y, Song W, Sharma A, Brunengraber H, and Sears JE (2019). Serine and 1-carbon metabolism are required for HIF-mediated protection against retinopathy of prematurity. JCI Insight 4, 1–12. 10.1172/jci.insight.129398.

81. Singh C, Hoppe G, Tran V, McCollum L, Bolok Y, Song W, Sharma A, Brunengraber H, and Sears JE (2019). Serine and 1-carbon metabolism are required for HIF-mediated protection against retinopathy of prematurity. JCI Insight 4, 1–12. 10.1172/jci.insight.129398.

Highlights

- Increases in hepatic cytosolic NADH/NAD^+ (reductive stress) change the hepatic transcriptome
- These transcriptional changes are mediated by ChREBP which is activated by reductive stress
- *GCKR's* metabolic pleiotropy is explained in part by ChREBP's activation via reductive stress
- Multiple human metabolic traits may be influenced by a GCKR-NADH/NAD+-ChREBP-FGF21 axis.

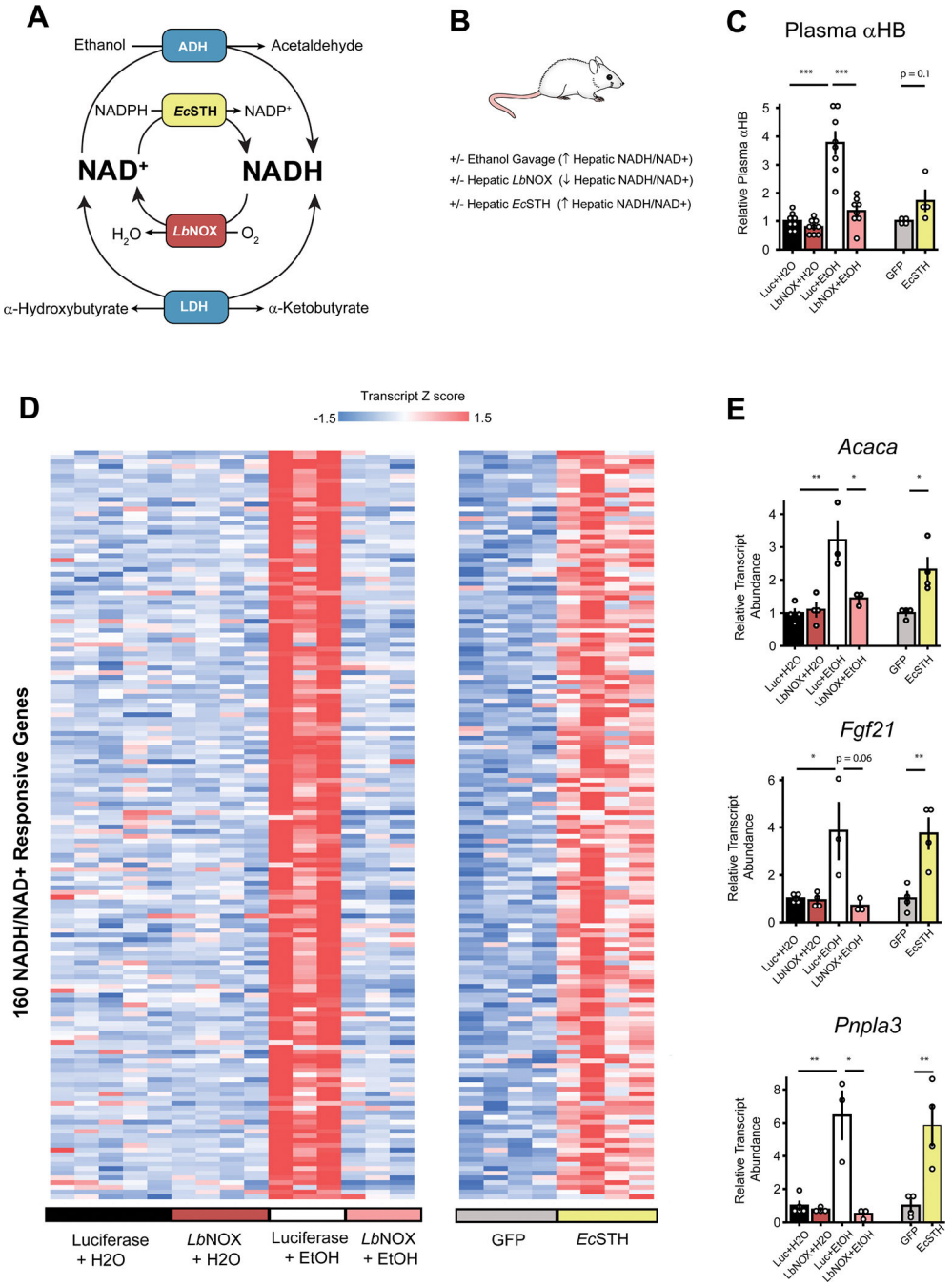

Figure 1. Increased cytosolic NADH/NAD$^+$ induces hepatic transcriptional changes.

(**A-B)** Schematic of the effects of *Lb*NOX, *Ec*STH, and ethanol on NADH and NAD$^+$ and α-hydroxybutyrate in the liver. **(C)** A combination of ethanol gavages, hepatic *Lb*NOX and *Ec*STH expression raises or lowers hepatic NADH/NAD$^+$ as measured by circulating α-hydroxybutyrate. *Lb*NOX/EtOH data was previously reported in reference 1. (**D**) Hepatic RNAseq demonstrates approximately 160 transcripts are NADH/NAD$^+$ responsive. **(E)** Examples of NADH/NAD$^+$ responsive genes include *Fgf21*, *Acaca*, and *Pnpla3*. Values

denote mean +/− s.e.m unless otherwise noted. n= 4–8 (C), 3–5 (D), or 4 (E) per group. * $p < 0.05$, ** $p < 0.01$; *** $p < 0.001$.

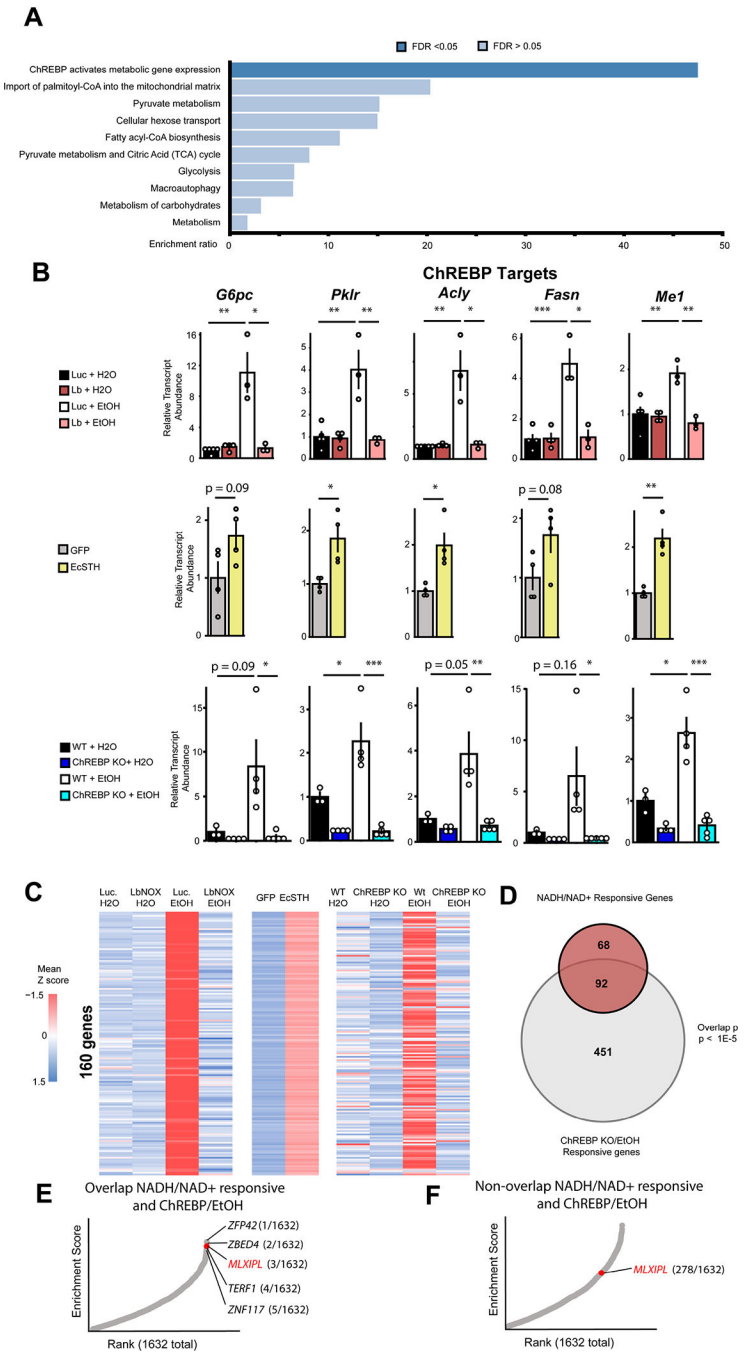

Figure 2: ChREBP mediates NADH/NAD+-dependent hepatic transcriptional changes:
(A) Overrepresentation analysis of NADH/NAD$^+$ sensitive transcripts identifies ChREBP-related pathways (**B**) Transcript abundance of ChREBP canonical targets *G6pc*, *Pklr*, *Acly*, *Fasn* and *Me*1 in the context of +/−*Lb*NOX +/−ethanol gavages (top row), *Ec*STH/GFP (middle row), and ChREBP WT/KO +/− ethanol gavage (bottom row) experiments. (**C**) Mean z-score of gene expression of NADH/NAD$^+$-responsive genes in different mouse experiments. (**D**) Overlap of NADH/NAD$^+$-responsive genes and ChREBP/ethanol responsive genes. **(E)** Chea3 transcription factor enrichment analysis (TFEA) of 1632

transcription factors in the overlapping (N=116 genes) and (**F**) non-overlapping NADH/NAD+ and ChREBP/EtOH responsive gene sets. Data are mean +/− s.e.m unless otherwise noted. n=3–5ewawd.* $p < 0.05$, ** $p < 0.01$; *** $p < 0.001$.

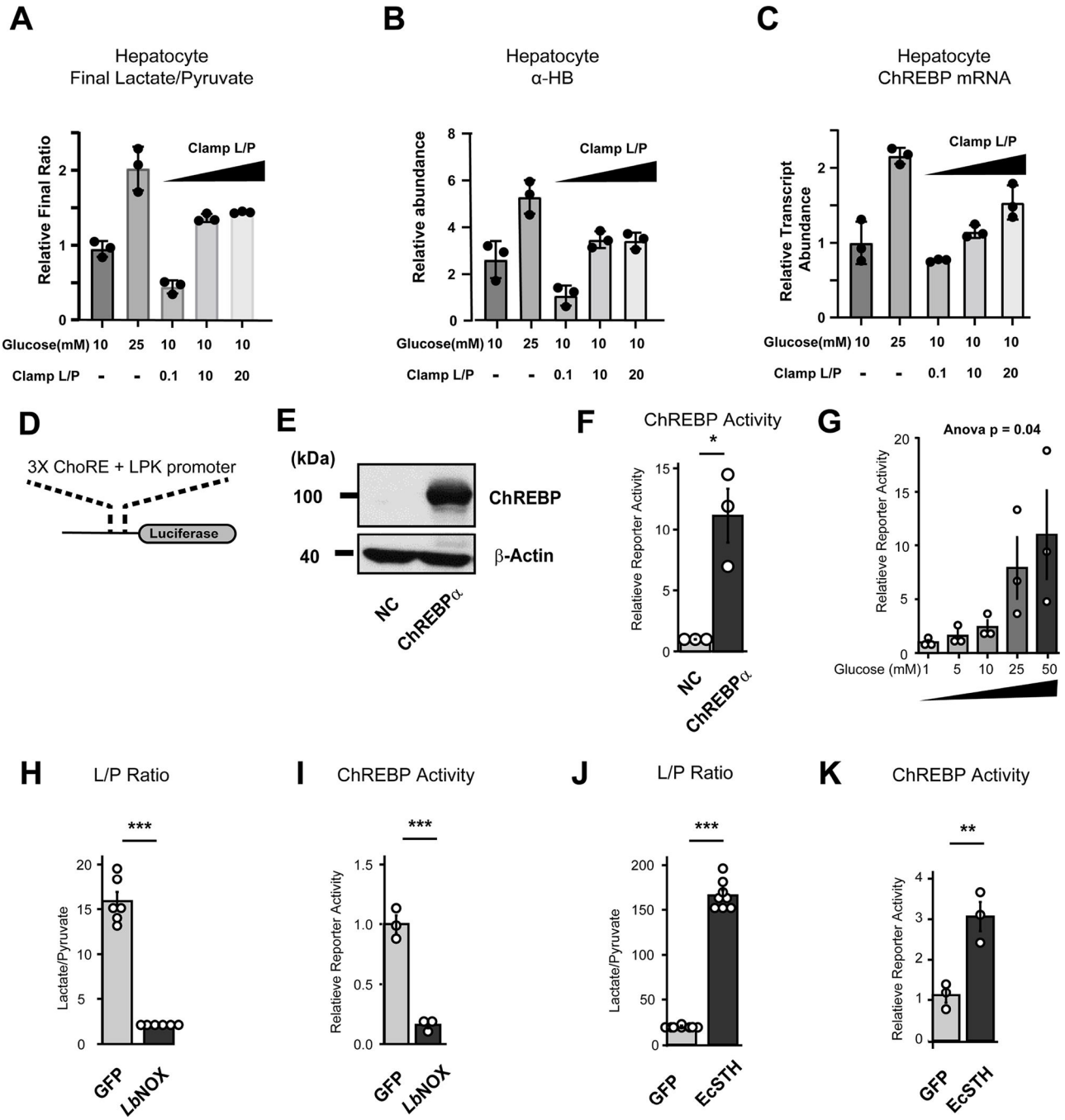

Figure 3: Elevated cytosolic NADH/NAD$^+$ activates ChREBP.

Relative **(A)** final lactate/pyruvate ratio, (**B)** αHB, **(C)** ChREBP mRNA in primary hepatocytes from n=3 mice with different clamped media lactate/pyruvate ratios. **(D)** Design of a ChREBP/luciferase reporter construct. (**E**) ChREBP expression in 239T cells, with **(F)** relative luciferase activity with and without ChREBP and **(G)** with different glucose concentrations. **(H)** Effect of *Lb*NOX expression on media lactate/pyruvate ration and (**I)** ChREBP activity. (**J**) Effect of *Ec*STH on media lactate/pyruvate levels and (**K**) ChREBP activity in HEK 293T cells. *P* values were determined using unpaired, Student's t test (**F, H,**

I, K, L) or one-way ANOVA (**G**). Data are mean +/− s.e.m unless otherwise noted. * $p < 0.05$, ** $p < 0.01$; *** $p < 0.001$. n=3 for all experiments except for H (6) and J (7).

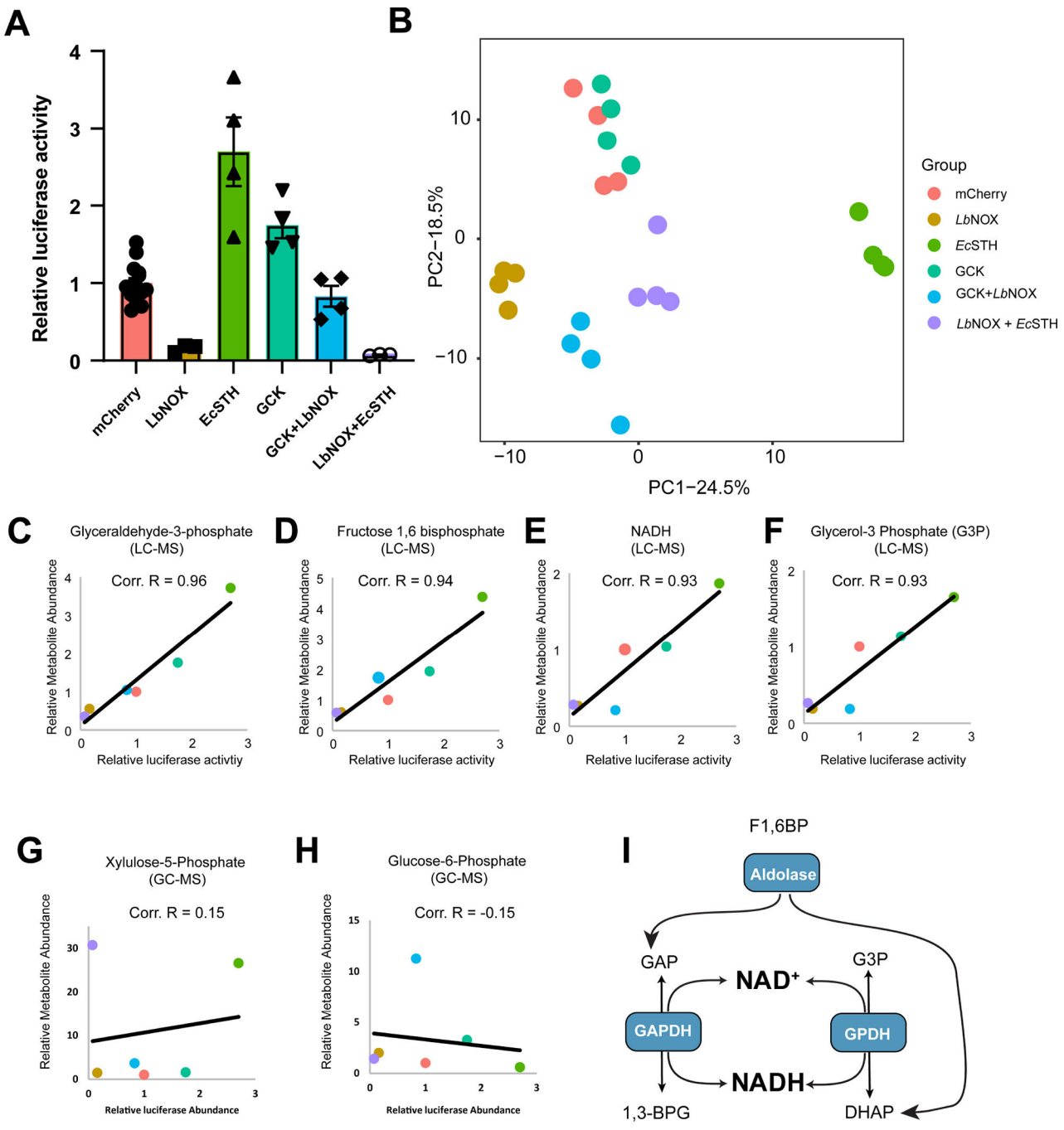

Figure 4: Metabolic perturbations of ChREBP activity correlate with intracellular phospho esters.

(**A**) Luciferase activity of ChREBP reporter system after transfection with different metabolic enzymes. (**B**) PCA of intracellular metabolites. Correlation of intracellular (**C**) Glyceradehyde-3-phosphate, (**D**) Fructose 1,6-bisphopshate, (**E**) NADH, and (**F**) Glycerol-3-phosphate. (**G**) Xylulose-5-phosphate, (**H**) Glucose-6-phosphate. (**I**) Intracellular NADH/NAD$^+$ are linked to F1,6BP, GAP, and G3P via the dehydrogenases GAPDH and GPDH. Data are mean +/− s.e.m unless otherwise noted. n=4 for all experimental groups.

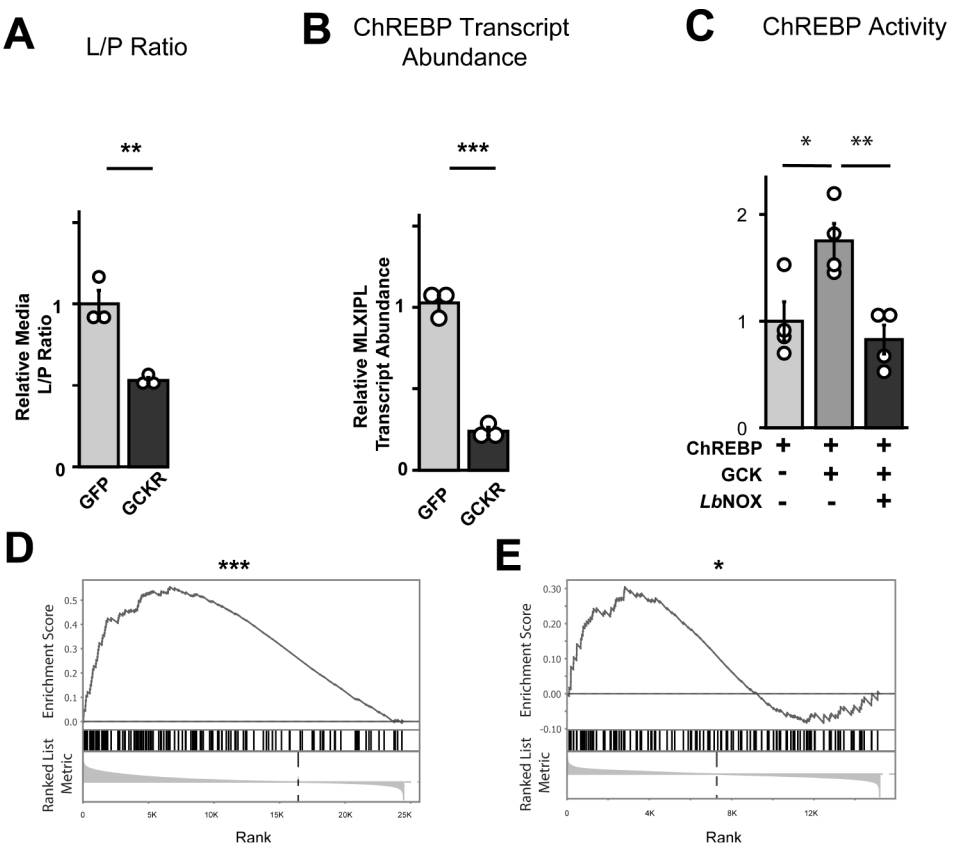

Figure 5: Effect of *GCKR and GCK* on ChREBP and NADH/NAD$^+$.

Effect of GCKR overexpression on (**A**) media lactate/pyruvate ratio and **(B)** ChREBP transcript abundance in HepaRG cells. **(C)** Effect of GCK expression with and without *Lb*NOX on ChREBP reporter activity in HEK 293Ts. (D) Preranked GSEA of the NADH/NAD$^+$ response gene set in RNA-Seq with TT versus CC genotypes in human liver biopsies and (E) human liver organoids with different GCKR gneotypes[33]. Data are mean +/− s.e.m unless otherwise noted. * $p < 0.05$, ** $p < 0.01$; *** $p < 0.001$. n=3 (A,B,D), 4 (C), or 9 (E).

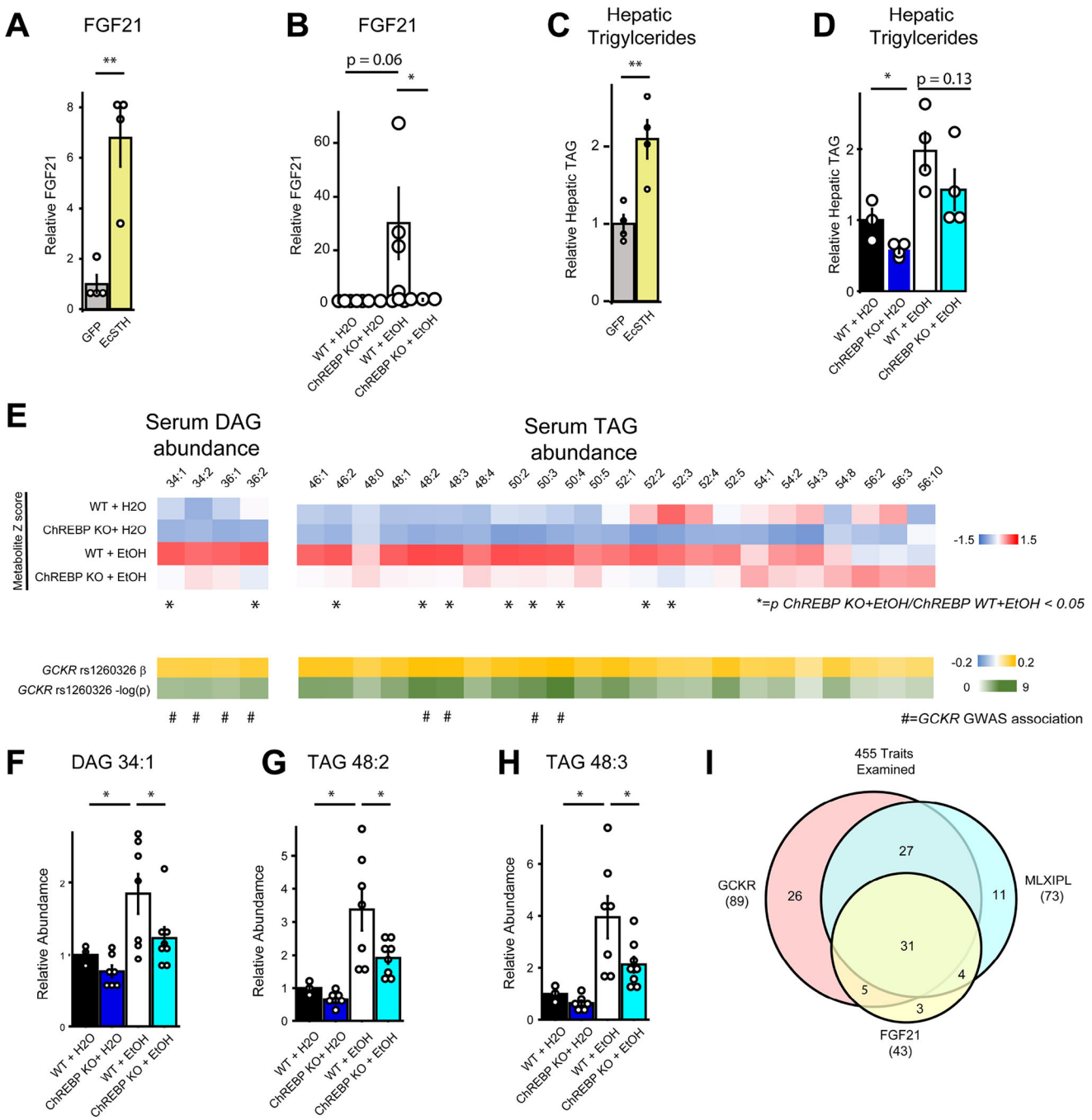

Figure 6: *Ec*STH and ChREBP influence *GCKR*-associated metabolic traits.

Circulating FGF21 is influenced by hepatic EcSTH (**A**) and ethanol via ChREBP (**B**) as are hepatic triglycerides (**C** and **D**). **E (top):** Serum triglyceride species Z score by genotype and gavage, (**bottom**) p and b value of effect of *GCKR* rs1260326 on triglyceride species taken from reference[69]. * indicates TAG species formally linked to *GCKR* genetic variation in human GWAS studies. (**F-H**) Specific TAG species associated with *GCKR* rs1260326 in humans and the influence of alcohol and ChREBP on its abundance. **(I)** Overlap of *GCKR*,

FGF21, or *MLXIPL* influenced traits from Type 2 Diabetes Knowledge Portal. Data are mean +/− s.e.m unless otherwise noted. * $p < 0.05$, ** $p < 0.01$; *** $p < 0.001$.

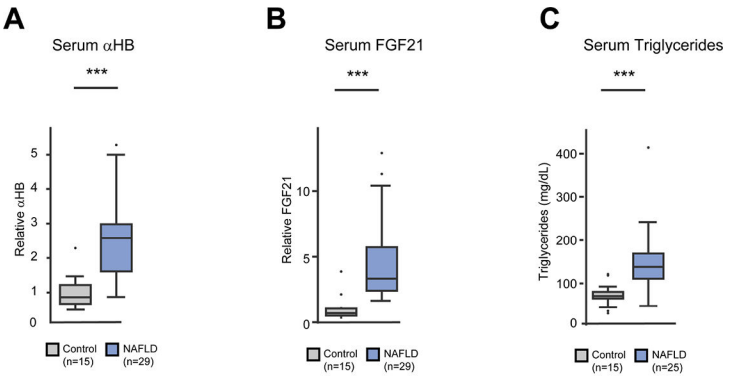

D

GSEA of NADH/NAD+ responsive genes in Human Liver Genomic Data sets

Gene Set	Cohort	NADH/NAD+ responsive GSEA Enrichment Score	NADH/NAD+ responsive GSEA Enrichment P value
GSE130970	NAFLD/No NAFLD	1.31	0.001
dbGAPphs001807	NAFLD/No NAFLD	1.28	0.03
GSE135251	NAFLD/No NAFLD	1.78	<0.001
GSE48452	Bariatric Surgery	1.4	0.004
GSE83452	Bariatric Surgery	1.4	0.02
E-MTAB-11688	NAFLD/No NAFLD after liver transplant	1.58	<0.001

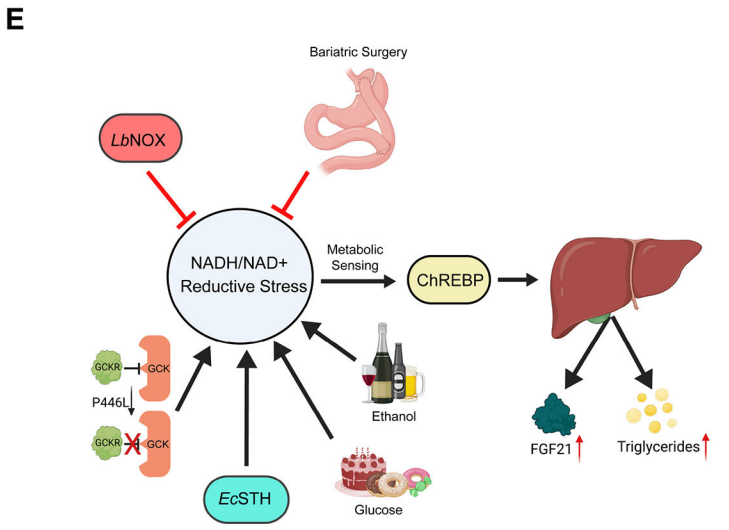

Figure 7: αHB, FGF21, serum triglycerides, and the transcriptional signature of hepatic reductive stress is increased in patients with fatty liver disease

(A) Serum αHB, (**B**) FGF21, and (**C**) triglycerides are elevated in patients with NAFLD compared to healthy controls. p values calculated from Welch's t-test. (**D**) The transcriptional signature of reductive stress is upregulated in multiple human liver genomic data sets of patients with NAFLD. In the box and whisker plots the horizontal line represents the median, the top and bottom of the box are the 75th and 25th percentile, respectively, and the top/bottom error bars reflect the largest/smallest value within 1.5 times of the

interquartile range beyond the $75^{th}/25^{th}$ percentile. *** $p < 0.001$. (E) Proposed model describing how hepatic NADH/NAD+ influences metabolic traits.

Key resources table

REAGENT or RESOURCE	SOURCE	IDENTIFIER
Antibodies		
ChREBP Novus	Novus	NB400-135
Beta Actin	Cell Signaling technology	4970; RRID: AB_2223172
Goat anti-Rabbit IgG, HRP	Invitrogen	31460
Bacterial and virus strains		
EcSTH adenovirus	Vector Biolabs	Ad-CMV-EcSTH-Flag Lot no-20230420#1
GFP adenovirus	Vector Biolabs	Ad-GFP Lot no-20230309#1
Biological samples		
Human blood samples	MGH NAFLD Repository[79] and Partners Biobank.	NA
Chemicals, peptides, and recombinant proteins		
Sodium lactate	Sigma Aldrich	L7022
Sodium pyruvate	Sigma Aldrich	P5280
Liberase TM	Sigma Aldrich	LIBTH-RO
O-(2,3,4,5,6-Pentafluorobenzyl)hydroxylamine hydrochloride	Alfa Aesar Chemicals	A18368.03
Methanol	Fisher Chemicals	A456-4
Glutamax	Gibco	35050061
Penicillin-Streptomycin (10000 U/ml)	Gibco	15140122
HepaRG Growth Medium	Biopredic	ADD711C
HepaRG Differentiation Supplement	Biopredic	ADD721C
D-Ribose 5-phosphate disodium salt hydrate	Sigma Aldrich	R7750-10MG
DL-alpha-Glycerol phosphate magnesium salt hydrate	Sigma-Aldrich	17766-50G
D-Xylulose 5-phosphate lithium salt,≥90% (TLC)	Sigma-Aldrich	15732-1MG
Genticin	Gibco	10131027
Protease/phosphatase Inhibitor Cocktail (100X)	Cell Signaling Technology	5872S
Applied Biosystems TaqMan Fast Advanced Master Mix	Applied Biosystems	44-445-57
Iscript™ gDNA Clear cDNA Synthesis Kit	Bio-Rad	1725034
Pyridine, for HPLC, ≥99.9%	Sigma Aldrich	270407-100ML

REAGENT or RESOURCE	SOURCE	IDENTIFIER
Ethanol, Absolute (200 Proof), Molecular Biology Grade, Fisher BioReagents	Fisher Scientific	BP2818-500
Fetal Bovine Serum	Gibco	26-140-079
Agilent DB-5MS 30m, 0.25mm, 0.25um, 10m DRGRD - JW	Agilent Technologies	122-5532G
Agilent DB-1 30m, 0.25mm, 0.25um, 10m DRGRD - JW	Agilent Technologies	122-1032G
Itaq™ Universal SYBR	Bio-Rad	1725121
William's E Medium, no glutamine	Thermo Scientific	12551032
OPTI-MEM	Gibco	31985-062
0.25% trypsin-EDTA	Gibco	25200-056
RIPA buffer	Boston BioProducts	BP-115
Tris Buffered Saline-Tween	Boston BioProducts	IBB-180
Western Lightning Plus-ECL	PerkinElmer	NEL105001EA
Dulbecco's Modified Eagle Medium	Gibco	11995-065
Critical commercial assays		
ELISA FGF21 mouse/rat	Sigma Aldrich	EZRMFGF21-26K Lot no# 3280681
RNeasy mini kit	Qiagen	74004
SuperScript III First-Strand Synthesis System	Invitrogen	12574026
Firefly & Renilla Luciferase Single Tube Assay Kit	Biotium	30081-1
Lipofectamine 3000 Transfection Reagent	Invitrogen	L3000008
QIAprep Spin Miniprep Kit	Qiagen	27106
Glycogen Assay Kit (ab65620)	Abcam	ab65620
Deposited data		
RNAseq data	This paper	GEO: GSE227264, GSE227057, and GSE237068
Experimental models: Cell lines		
HepaRG	Biopedic inc	HPR101
Human: 293T cells	ATCC	CRL-3216
Experimental models: Organisms/strains		
Mouse C57BL6J	Jackson Lab	Jackson lab Stock ID 000664
Mouse ChREBP KO	Lizuka et. al. 2004	Jackson lab Stock ID 010537

REAGENT or RESOURCE	SOURCE	IDENTIFIER
Oligonucleotides		
Human ChREBP Fwd: 5'-CAGACAGCAACAAGACCGAG-3'	Integrated DNA Technologies	NA
Human ChREBP Rev: 5'-GTCAAACCCCAGCTTGATGT-3'	Integrated DNA Technologies	NA
Human GAPDH Fwd: 5'-GCTCTCTGCTCCTCCTGTT-3'	Integrated DNA Technologies	NA
Human GAPDH Rev: 5'-GCGCCCAATACGACCAAAT-3'	Integrated DNA Technologies	NA
Human β-actin Fwd: 5'-AGAAAATCTGGCACCACACC-3'	Integrated DNA Technologies	NA
Human β-actin Rev: 5'-AGCACAGCCTGGATAGCAA-3'	Integrated DNA Technologies	NA
Mouse β-actin Fwd: 5'-TACTCTGTGTGGATCGGTGG-3'	Integrated DNA Technologies	NA
Mouse β-actin Rev: 5'-TCGTACTCCTGCTTGCTG AT-3'	Integrated DNA Technologies	NA
Mouse HPRT and ChREBP quantitech primer assays	Qiagen	Mm_Hprt_1_SG QT00166768 and Mm_wbscr14_1_SG QT00125335 respectively
Recombinant DNA		
pGL4.14[luc2/Hygro]	Promega	E669A
pGL4.75[hRluc/CMV]	Promega	E693A
pcDNA3.1-eGFP	Addgene	129020
pcDNA3.1-mCherry	Addgene	128744
pcDNA3.1-ChREBPα	Addgene	211754
pcDNA3.1-Mlxγ	Addgene	211755
pcDNA3.1-LbNOX	This paper (derived from addgene 75285)	NA
pcDNA3.1-EcSTH	This paper	NA
pLJM1-GCK	Addgene (derived from Addgene 20492)	NA
Software and algorithms		
GraphPad Prism	Dotmatics	Version 10
Bio Render	BioRender	NA
R	The R Foundation for Statistical Computing	Version 4.2.2
Other		
Chow	Prolab	Isopro RMH 2000 5p75
Tricarballic acid	Sigma Aldrich	T53503
Triglyceride assay kit	Sekisui Diagnostics	Sekure 236-60
Methoxyamine	Sigma Aldrich	226904
MSTFA + 1% TMCS	ThermoFisher	TS48915
Immobilon®-P PVDF Membrane	MilliporeSigma	IPVH00010